# A New Source of Lithium: Probing Massive Post Main Sequence Low-Metallicity Stars in Young Globular Clusters

Project Supervisors: Dr. Dorottya Szécsi & Prof. Ilya Mandel
Project Partner: Sam Ratcliff

**Nicholas James Bennett**

Student ID: 1332457
Word Count: ~8600

**Abstract:**
Globular clusters are dense concentrations of $\sim 10^5$ — $10^6$ stars with similar ages, typically $\gtrsim$ 10 Gyr. They provide a unique look at the evolution of stars. Due to the age of the stars present in globular clusters many are remnants of much older populations. While we expect levels of light elements to be consistent with population II stars, several observations show anomalies in the expected levels of lithium in the surface of some of these stars as well as other elemental abundances. We attempt to explain these results using evolutionary models of massive low-metallicity stars in the range of 45-100 $M_\odot$. The results show promise, with models displaying a large amount of lithium produced during the post-main sequence phase of evolution. This lithium, produced by the pp-chain during hydrogen shell burning in the post-main-sequence, is then mixed up by the deep convective envelope before the hot temperatures can destroy it. When the lithium reaches the surface layers of the star it can then be ejected by stellar winds or stripped by a nearby object or binary companion. We discuss the effect of changing initial mass and initial rotational velocities on the production mechanism. We find the most lithium production occurs in a model with initial mass 80 $M_\odot$ and initial rotational velocity $100 kms^{-1}$. We discuss whether this mechanism for production is sufficient to completely account for lithium abundances observed. We expect that by answering these questions, stellar models will be refined to match observations thereby removing uncertainties associated with massive stellar evolution at low-metallicity and the rapidly advancing field studying the evolution of globular clusters as a whole.

A thesis presented for the degree of
Physics and Astrophysics MSci


UNIVERSITY OF BIRMINGHAM

School of Physics and Astronomy and Institute of Gravitational Wave Astronomy
The University Of Birmingham
United Kingdom
March 2018

## Contents

# 1 Introduction

## 1.1 Big Bang Nucleosynthesis

Nucleosynthesis refers to the production of nuclei/elements from smaller constituents by nuclear fusion. For heavy elements such as oxygen, carbon and metals etc. this occurs in stellar cores, supernovae and more recently discovered to take place in in neutron star mergers or kilonovae (Kasen et al , 2017). For the smallest and lightest elements, however, namely isotopes of hydrogen, helium and trace amounts of lithium, this occurred in the first few seconds to minutes after the Big Bang. This is known as Big Bang Nucleosynthesis (BBN) and has many physical and observational justifications. The relative abundance of helium ($^4$He, $^3$He), deuterium (D) and lithium ($^7$Li) demonstrates that the mechanism for primordial nucleosynthesis is well understood.

Shortly after the Big Bang, the temperatures involved were so large that it took time for anything we recognise today as matter to form. As the universe began to expand and cool a quark-gluon plasma formed. As the universe continued to expand and cool the formation of baryons (neutrons and protons) from quarks, as well as leptons (electrons and neutrinos) could occur. When the universe was only a fraction of a second old and had cooled to $10^{10}$ K the formation of these particles stopped, starting the so called freeze out. This fundamental change in environment meant that the reversible reaction that forms protons from neutrons (shown below)(Villante & Dolgov , 2003) slowed and shifted the equilibrium to the proton forming reaction. This gave rise to a change in the ratio between neutrons and protons with a larger number of protons present than neutrons.

$$n + e^+ \Longleftrightarrow \bar{\nu_e} + p \tag{1}$$

$$n + \nu_e \Longleftrightarrow p + e^- \tag{2}$$

The universe expanded and cooled further to $10^7 K$ and with an age of around 3 minutes it was cool enough to allow the protons and neutrons to fuse, forming D, $^4$He (two D nuclei) and trace amounts of $^7$Li (a D and a T nucleus). Electrons then bound to the nuclei forming elemental H, He and Li etc.

## 1.2 Stellar Nucleosynthesis

### 1.2.1 PP Chains

Stellar nucleosynthesis, supernovae and kilonovae account for all other elemental production not due to BBN. This includes a fraction of the helium we see today as well as the heavier elements that are not primordial. In stellar cores fusion of hydrogen into helium is the first energy producing mechanism that not only keeps the star from collapsing, due to the balance between gravity and the radiation and hydrodynamical pressure, but also produces some of the helium we observe in the Universe. In stars, the main channels through which hydrogen is fused into helium is different to that of BBN, where two deuterium nuclei fuse, as the abundance of deuterium is too low. For Sun like stars, whose cores have temperatures below $10^7 K$, the main channels are the Proton-Proton or PP chains. These chains start with the fusion of two hydrogen nuclei to a deuterium nucleus with the release of a positron and an electron neutrino conserving charge and lepton number. The deuterium then further fuses with another hydrogen to produce a helium 3 nucleus as well as gamma radiation. From here the chain branches into two channels. A schematic diagram of the chains is shown in Figure.1 with relative percentages of how much these account for the overall production.

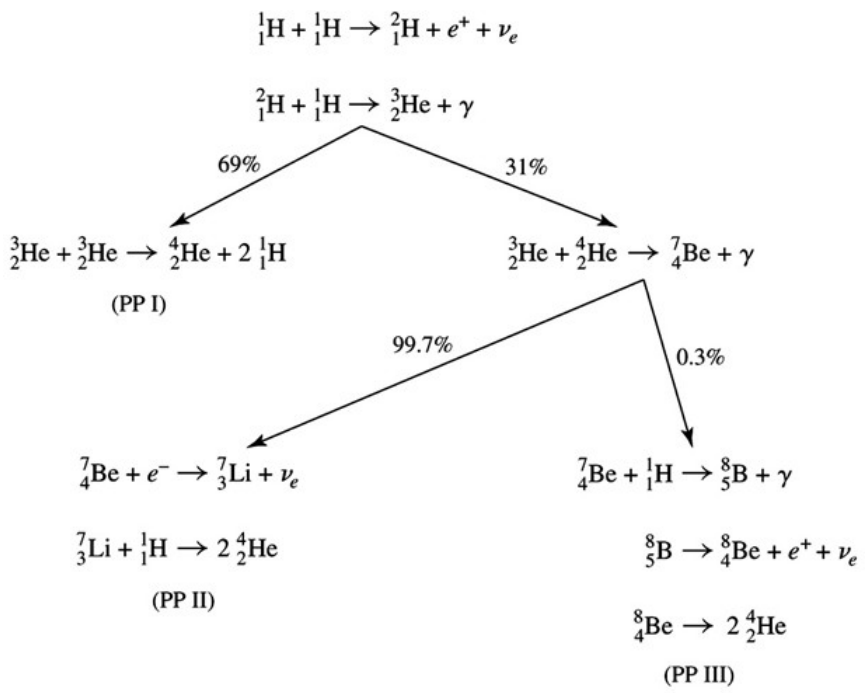


Figure 1: Chains of nuclear reactions that make up the PP process, the different chains are labelled with I, II, and III with the relative amount of the products used in subsequent reactions shown as a percentage.

The most important chain in this diagram is the PP I chain due to it accounting for $\sim 70\%$ of helium production with the PP II chain responsible for almost all the rest (PP III chain only accounts for $\sim 0.1\%$ of helium production). In Figure. 1 the bottleneck of the reaction is the very first step in the chain, where two hydrogen nuclei fuse. The relatively small cross-section of the proton leads to a slow rate of production of D. Additionally, once a D nucleus has formed it can then be destroyed before it captures a proton to form $^3$He. This leads to on average a proton waiting a billion years to undergo fusion. At high enough temperatures ($> 8 \times 10^6 K$) the other steps in this process have much shorter average times when compared to the initial reaction and so are not affecting the rate to any significant extent. At lower temperatures, however, the $^3$He + $^3$He reaction may affect the rate due to the need for a large amount of this isotope to form before reactions can take place.

For this investigation we note that the PPII chain can both destroy and form lithium. Firstly the second step in this chain consists of a $^7$Li capturing a proton and producing two $^4$He nuclei. In most stars this process is what is responsible for destroying much of the lithium present from the primordial levels. The first step is also important in that it provides a lithium production mechanism via the electron capture of a $^7$Be nucleus. This is an important mechanism in high mass, low-metallicity stars.

### 1.2.2 CNO Cycle

In more massive stars, where the core temperature is much higher ($> 10^7 K$), another process becomes the main channel through which helium is produced. The CNO cycle (Carbon-Nitrogen-Oxygen) is a long string of reactions that uses carbon, nitrogen and oxygen (and fluorine) as catalysts to produce helium. The star requires the presence of these catalysts from a previous generation of stars which produced these heavier elements meaning the initial composition of that star can have a significant effect on the dominance of these reactions. The PP cycle is still present in larger stars, however, the temperature dependence of both the CNO cycle and pp chains means the CNO cycle dominates at higher temperatures.

The CNO cycle and the PP chains have different temperature dependence leading to very different rates at the ranges of core temperatures of stars. In relatively low mass, cool stars like the Sun, or in

hydrogen burning shells, the PP chain dominates. At higher temperatures, where the stars are of order 1-2 magnitudes more massive than the sun, the CNO cycle dominates. The temperature dependences of these reactions are $\epsilon_{pp} \propto X^2 \rho T^4$ for the PP chains and $\epsilon_{CNO} \propto X X_{14} \rho T^{18}$, where $\epsilon_{pp}$ and $\epsilon_{CNO}$ is the energy generation of the PP chains and the CNO cycle respectively, $\rho$ is the density of the material, T is temperature and $X$ and $X_{14}$ are the relative abundances of He and $^{14}$N respectively. These values are included in the equation as they are involved in the bottleneck reaction. These relationships show that the CNO cycle has a much higher temperature dependence with an exponent of 18 to the PP chains 4, which results in the dominance of the CNO cycle for energy production at higher temperatures. A graphical representation of the temperature dependence is shown in a log-log plot of energy production vs stellar (core) temperature (Figure 2). The figure is taken from Ray (2009)

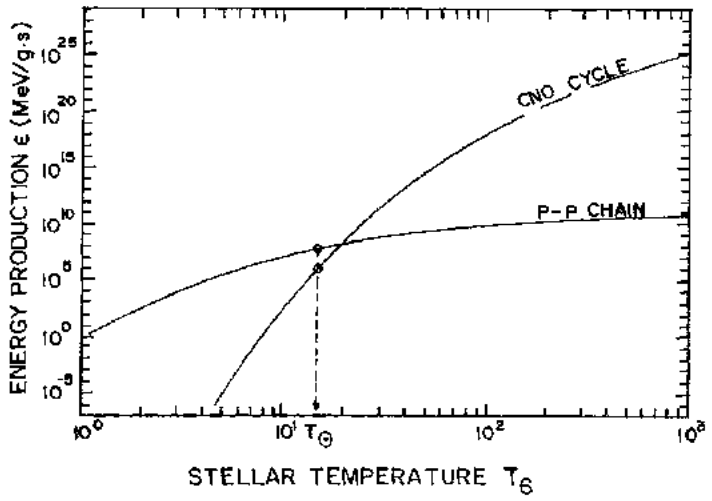


Figure 2: Energy production against core stellar temperature on a log-log plot for the PP chains and CNO cycle, solar values are indicated.

## 1.3 Stellar Clusters

Stellar clusters are fairly common objects in the Universe, indeed, our own galaxy provides many examples. There is considered to be 2 main types of star cluster, open clusters and globular clusters or (GCs). Open clusters are fairly young and their starts are in close proximity to each other due to them forming from the same large gas cloud. Open clusters are weakly gravitationally bound and can be disrupted fairly easily. These objects contain only a few hundred to a few thousand stars, being on average around 10 light years across. Globular clusters on the other hand can contain up to 1 million stars compared to a typical open clusters 1000. GC are also more dense with stars in the core having a density of 100 to 1000 per cubic parsec and the average distance being around 1 light year, stars in open clusters are typically less densely packed, especially in older clusters.

### 1.3.1 Globular Clusters

Globular clusters are massive objects and much more dense than open clusters. They are much more spherical and symmetrical in shape compared to open clusters and are much older. Most estimates for the average age are $\sim 12Gyr$ in (Krauss & Chaboyer , 2003) with the age of particular GCs such as M4 being $\sim 9Gyr$. These objects contain old stars which are up to few solar masses as more massive stars will have evolved more quickly and star formation rate in these objects is effectively 0. These more massive stars may have left behind remnants such as white dwarfs, neutron stars and black holes which can still contribute to the overall mass of the object. Globular clusters contain as many

as 1 million individual stars which are heavily bounded gravitationally to each other. Moreover, stars in most globular clusters are metal poor, so they are thought to have been some of the first stars that formed from the material left over after the Big Bang. The age and relatively low metallicity of many of the stars in globular clusters mean they are classified as population II stars. In the Milky Way and other galaxies, globular clusters are found in the halo and help to outline the outer limits of the galaxy. Most stars in globular clusters and red in colour as the cluster age means that only low mass stars are still burning and therefore observable, with most of them being in the red giant phase of stellar evolution. Some bluer stars exist in these clusters, they are in the horizontal stage of the evolution where a helium flash causes the star to become hotter and bluer. The stars in globular clusters have a variety of ages as there is thought to be multiple stellar formation stages during a clusters lifetime.

The formation of GC's is thought by some to be similar to that of open clusters, just on a larger scale and with the formation taking place long before that of any open cluster. There is evidence, however to suggest a similar mechanism may be problematic. Observations of nearby dwarf galaxies call into question the details of these models. One of the main issues is the idea that globular clusters would have to lose a large amount of their original mass, previously thought to be accounted for by ejection of stars into the surrounding space. This issue is debated by (Larsen et al , 2014) by looking at observation by Hubble of the dwarf galaxies WLM and IKN. The observations by Hubble do not support the idea of stellar ejection as the stars that would be expected from this process are not present. For the most part the formation of globular clusters is not clearly understood and there are many irregularities with the models presented and the observations. Furthermore, due to their age, it is difficult to wind back the clock as with open clusters and so the properties we infer have many caveats.

## 1.4 Multiple Populations

For many years astronomers have believed that globular clusters are comprised of a single generation of stars due to similarities between other clusters, such as open clusters. Many since (Piottio et al , 2012; Piotto et al , 2007; Villanova et al , 2007), however, have observed that GCs are comprised of more than one generation of stars, meaning the stars that GCs contain belong to multiple populations. The evidence of this multiplicity of generations is provided by photometric and spectroscopic observations. Stellar populations are defined by their similarities in both age and composition, namely the metallicity and He abundance, and they have masses distributed in accordance with the IMF (Salpeter , 1995). The two major pieces of evidence is that of main sequence multiplicity and correlations/anti-correlations between light elements, with the observational evidence in each case being photometric and spectroscopic respectively. Though GCs and their evolution are not widely understood, these observations show that over their lifetime GCs experience many star forming episodes, the effects of which are still observable today.

### 1.4.1 Main Sequence Multiplicity

Multiple populations in GCs would have a variety of observational consequences. Firstly, these populations have been observed to differ in age by 1-2 Gyr (Piottio et al , 2012) with other observations showing age differences of 4-5 Gyr (Villanova et al , 2007) therefore we expect the H-R diagram not follow the track of a single isochrone. Instead, we expect broadening or even clear splits in many areas of the colour-magnitude diagram (CMD). Many observations have shown that multiple main sequences are present in globular clusters. Multiplicity is also observed in red giant and sub-giant branches (Piottio et al , 2012). Some clusters such as NGC 2808, which show up to three separate main sequences (Piotto et al , 2007), give enormous credibility to the idea of multiple populations and show that many distinct star forming periods occur during the lifetime of GCs. This leads to the presence of multiple populations.

### 1.4.2 Light Element Anti-Correlations

Light elemental abundance provides a window into the interaction of different populations in the same GC. Their abundance as well as the anti-correlations between them give insight to the fate of previous generations. Enrichment of the stars that we currently observe has been used to explain spectroscopic results (Pasquini et al , 2005; Monaco et al , 2012; Bastian et al , 2013). Due to relative abundance of elements such as oxygen, sodium, magnesium and aluminium and their importance in proton capture, it can be concluded that high temperature hydrogen burning occurred in earlier generations of stars, possibly in high mass stars ($> 10M\odot$) (Matteucci et al , 2000). The Ne-Na and Mg-Al cycles that occur in massive stars produce some of these anticorrelations. These stars then, by some mechanism, polluted the subsequent generations leading to observations such as those in Monaco et al (2012) and Pasquini et al (2005). Relationships between Na and O give credence to these conclusions, such as the Na-O anti-correlations. These anti-correlations are signatures of high temperature H-burning. Such observations are made and analysed in Carretta et al (2009). This paper looks at the spectra of over 1400 red giants in 15 GCs. Using these observations it is possible to deduce that 3 distinct population categories exist. The first of these categories is a primordial population, characterised by low Na and high O as these stars formed from primordial material. The second and third categories are two sets of a second generation which are characterised by high Na and low O. Compositional differences in the observed stellar photosphere's and anti-correlations like these, along with high levels of Li in current stars, are evidence of multiple populations and of enrichment of the interstellar/intra-cluster medium.

## 1.5 Massive Star Evolution

Massive stars are not as common in the Universe as stars such as the Sun. Following the initial mass function of Kroupa (2001) it can be calculated that stars in the mass range $8M_{\odot} \leq M_{star} \leq 150M_{\odot}$ account for only 0.72% of the number of stars in a typical collection. These massive stars, however, account for $\sim 21\%$ of the mass. Because of this they are very important objects to study in the context of globular clusters, black holes and energetic processes such as supernovae. Massive stars are considered to be larger than $\sim 8M_{\odot}$. This mass is intrinsic to the latter stages of evolution, particularly burning of elements heavier than helium, the details of which will be discussed later. The upper limit on stellar mass is disputed, however, but stars of mass $\geq 150\ M_{\odot}$ have been observed in the certain clusters (Crowther et al , 2010). Stars more massive than this are hypothetical.

Massive stars have much shorter lifespans than lower mass stars. Their ages are generally in the range of 2-50 Myr. Massive stars go through their evolution much more quickly than lower mass stars and are larger and much more luminous. Due to their immense luminosity, mass loss due to winds is quite significant during the main sequence and indeed all stage of evolution. Mass loss is highly dependent on metallicity and mass with stars of high metallicity suffering from high mass loss. The envelope does not, however, experience mass loss in the same way as low-to-intermediate mass stars, in the form of a planetary nebula.

### 1.5.1 Formation and pre-main sequence

Much like any star, formation of massive stars begins as a weakly bound, cold and dense collection of gas and dust. This gas cloud or dark nebula then begins to collapse via an external trigger such as supernova shocks, gravitational perturbations or internal inhomogeneities in the structure or magnetic fields. As the gas collapses it begins to heat up as the molecules are in closer proximity to each other. A protostar slowly forms from this gas cloud and, as the cloud continues to collapse further, the core of this object heats up to $\sim 2.6 \times 10^6 K$, enough for hydrogen burning to begin. This process, while still occurring at high temperatures, is assisted by the quantum tunnelling effects which allow the core temperature to be a few orders of magnitude lower. When hydrogen burning begins, the radiation pressure produced by the nuclear processes causes most of the loosely bound gas and dust, not part of the star or surrounding satellites like planets, to be ejected into interstellar space. This is when

the object becomes a star.

### 1.5.2 Main-sequence

As the massive star evolves further it eventually begins the main sequence. While on the main sequence the star fuses hydrogen into helium mainly via the CNO cycle due to the high temperatures. Surface temperatures can be in the range $15,000K$ to $40,000K$ or more but core temperatures can exceed $6 \times 10^8 K$ during carbon burning.

In OB-type main-sequence stars mass loss is driven by radiation at spectral absorption line frequencies. As the atoms are accelerated the Doppler broadening allows these atoms to absorb photons of higher frequency and therefore higher energy. This mechanism causes positive feedback which allows the atoms in the wind to completely escape the gravitational pull of the star. However, observed levels of mass loss are generally less than this theory predicts. This is largely due to wind clumping which can decrease the observed mass loss by 2 to 10 times (Puls et al , 2008). At the highest masses, stars can exhibit nebulosity due to the ionisation of ejected material.

### 1.5.3 Post Main-sequence and star death

Once a helium core is formed hydrogen shell burning continues adding more helium to the core. As the core is not degenerate i.e. electron degeneracy pressure does not support the star, helium burning can eventually occur steadily. Helium burns by means of the triple alpha process (Oberhummer et al , 1999) to form beryllium and then carbon. This is unlike low mass stars which undergo helium flash due to the degenerate core. The time frame of the main sequence of a massive star is in the order only a few million to a few tens of millions of years. The post-main-sequence of massive stars differs greatly from that of low and intermediate mass stars as the burning of nuclear fuel can continue. Even after core-helium-burning, massive stars have non-degenerate cores and can ignite $^{12}$C present in their cores. The $^{12}$C fuses with $^4$He nuclei via helium capture to produce $^{16}$O. Similarly $^{16}$O and $^{20}$Ne also fuse via this channel fusing with $^4$He to produce $^{20}$Ne and $^{24}$Mg respectively. Larger stars still can fuse heavier elements up to iron.

Fusion of Fe is endoenergetic due to it having the largest binding energy per nucleon of any element. More energy is needed to fuse Fe than is released in this reaction. As Fe cannot be fused inside a star it builds up in the core with successive layers of lighter elements including Si, Ne, Mg and O. Eventually the core cannot sustain itself through fusion so it becomes degenerate , the $e^-$ pressure is then not enough to prevent collapse. oncer the Chandrasekhar limit of core mass ($\sim 1.4 M_\odot$) (Chandrasekhar , 1931) is reached the core collapses and the star explodes as a supernova. For stellar cores of mass $1.5 M_\odot$ to $3 M_\odot$ a dense neutron star is formed while for cores more massive that this the collapse is unimpeded with much of the energy absorbed by processes such as photo-disintegration and electron capture via inverse beta decay. A black hole is formed.

### 1.5.4 The Kippenhahn Diagram

The Kippenhahn diagram is a 2 dimensional plot that indicates boundaries between different parts of star and how these evolve over time. The layers are qualitatively distinct and usually show areas of convection, semi-convection, convective overshoot and nuclear burning. Kippenhahn diagrams show convection and nuclear energy generation as these effect and phenomena are generally indicative of distinct shells. Kippenhahn diagrams are generally used when presenting data created in stellar simulations as they allow areas of interesting and important physics to be visualised from raw output.

## 1.6 Binary Mass Transfer

A binary star system, which consists of two stars orbiting a common centre of mass, occurs often for massive stars. During the lifetime of these stars, mass can be transferred from one star to another.

This occurs when matter previously bound to a star extends out of the stars Roche lobe, meaning it is not gravitationally bound to the star. There are three different types of mass transfer in binary systems. These are known as Case A, B and C and differ at the stage of mass transfer. Case A refers to mass transfer that occurs when the donor star is still on the main sequence. Case B refers to mass transfer during the donor stars evolution into the red-giant or red-supergiant. Case C refers to the mass transfer when the donor star is in the red-giant or supergiant phase. The mass transfer can be either conservative or non-conservative. In conservative mass transfer the matter is conserved within the system rather than being ejected from the system such as in non-conservative mass transfer. The timescale upon which the mass transfer occurs depends on a number of factors. Firstly, the mass-radius is dependent on the age of the star and its composition. For zero age main sequence stars a particular relationship is used, whereas for stars coming to the end of the main sequence, the radius can rapidly increase. For the latter situation mass loss can be considered to occur on thermal timescales as simple mass loss is not enough to reduce the radius to below the Roche lobe. The properties of the envelope must also be considered when discussing timescales. For a radiative envelope only a small amount of mass needs to be lost before the star is no longer in thermal equilibrium and a thermal timescale is required to bring the star back into thermal equilibrium. For convective envelopes such as the envelopes present in massive stars in the post main sequence the mass loss rate occurs on hydrodynamic timescales as material is continually circulated in the envelope.

# 2 Methods, Results and Analysis

## 2.1 Motivation: The Lithium Problem

Globular Clusters, whilst fairly common in our galaxy and many others, are not well understood in terms of their evolution. Observations of a few different globular clusters (Pasquini et al , 2005; Monaco et al , 2012) show high levels of lithium in the surface of some of these stars, while most other stars exhibit abundances of $A(Li) \sim 1$ (D'Orazi et al , 2015). Some attempt to explain these abundances using AGB stars (Pasquini et al , 2005) or other mechanisms (Bastian et al , 2013). These clusters also exhibit star-to-star variations in certain elements leading to the conclusion that they must have been formed from gas enriched by a previous generation of massive stars. Given that in massive stars primordial lithium produced in the Big Bang is destroyed during the main sequence, it does not seem that any lithium should be observed in these stars. This leads to the question: Is there a new source of lithium in the Universe?

## 2.2 Lithium Production in Massive Stars

We have used models produced in Szécsi et al (2015) which used the binary evolution code (BEC), details of which can be found in section 2 of that paper and in the appendix A.3. The models examined closely were of massive low-metallicity stars. We firstly analysed models with initial masses of 45 $M_{\odot}$, 77 $M_{\odot}$ and 100 $M_{\odot}$ with each having an initial surface rotational velocity of $100 kms^{-1}$ as well as a composition of 0.1 times that found in the Small Magellanic Cloud which corresponds to $\sim \frac{1}{50}\ Z_{\odot}$. The models were run from zero age main sequence to core helium exhaustion. By studying these models we were able to see how much lithium was present over their lifetimes as well as where this lithium was concentrated. The surface lithium abundance was plotted for each model. It shows an expected depletion of lithium during the main sequence, however, during the post main sequence a large and sudden increase in the lithium abundance is seen. Details of the abundances units used in this investigation can be found in the appendix A.1.

### 2.2.1 Lithium surface levels

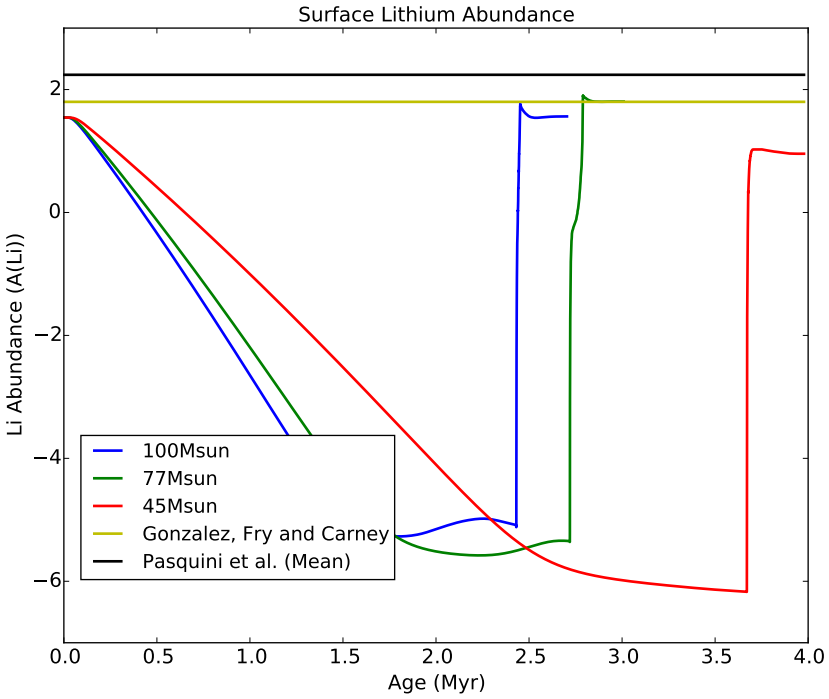


Figure 3: Lithium surface abundances over the lifetime of the stars. Each model is shown in a different colour which is indicated. Reference levels for observations by Carney, Fry and Gonzalez (1998(@) and Pasquini et al (2005) are shown.

### 2.2.2 Correlations and Anti-Correlations

As discussed in section 1.4.2, if we are to assume the observed stars with high lithium abundance were formed from material polluted by massive stars from a previous generation, we should be able to observe similar correlations and anti-correlations in our models as in the observed stars (Pasquini et al , 2005; Monaco et al , 2012). We created plots showing the changes in certain elements at the surface pertinent to high temperature nuclear processes, i.e. in the cores of massive stars. The nuclear burning products are mixed between core and surface over the main-sequence lifetime of the models by rotational mixing.

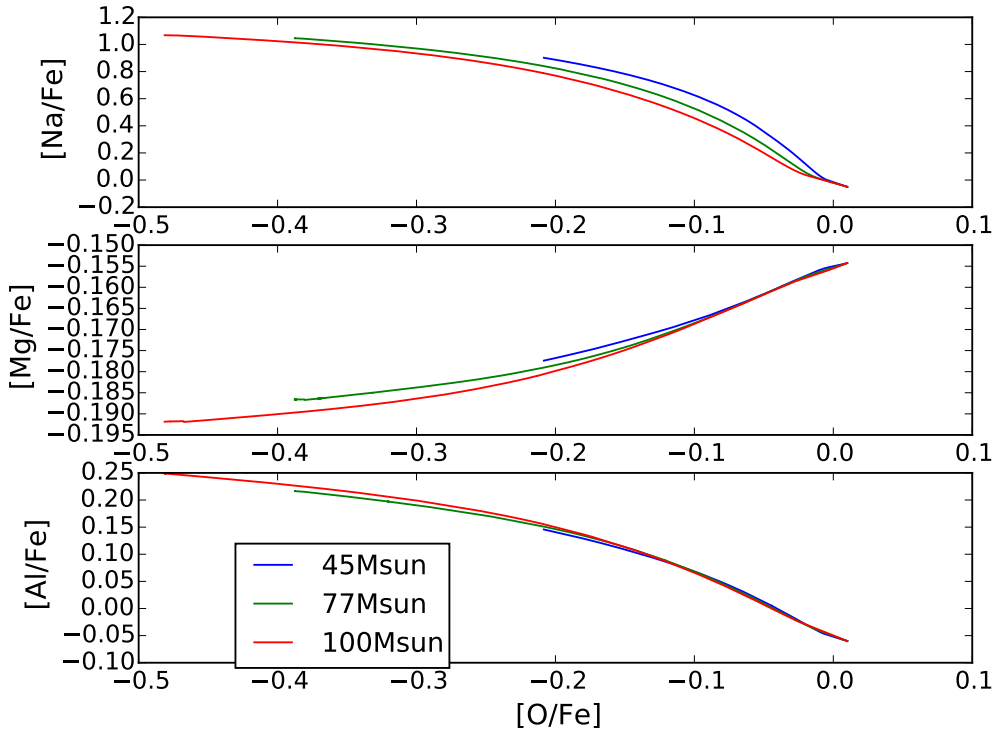


Figure 4: Oxygen surface abundance vs sodium [Na/Fe], magnesium [Mg/Fe] and aluminium [Al/Fe] for the entire lifetime of models of initial mass 45 $M_{\odot}$, 77 $M_{\odot}$ and 100 $M_{\odot}$.

We found that the surface composition of the models exhibit correlations and anti-correlations. Thus if a second generation of low mass stars were to form out of this material, they would be expected to follow these elemental ratios. We have computed models between initial masses of $45 - 100$ $M_{\odot}$. Figure 5 shows the highest surface levels of lithium compared to both oxygen and nitrogen. While the levels of lithium produced in our models are quantitatively close to those observed in Pasquini et al (2005); more research is required to establish how the observed correlations between lithium and oxygen, as well as lithium and nitrogen can be explained by our models, if at all.

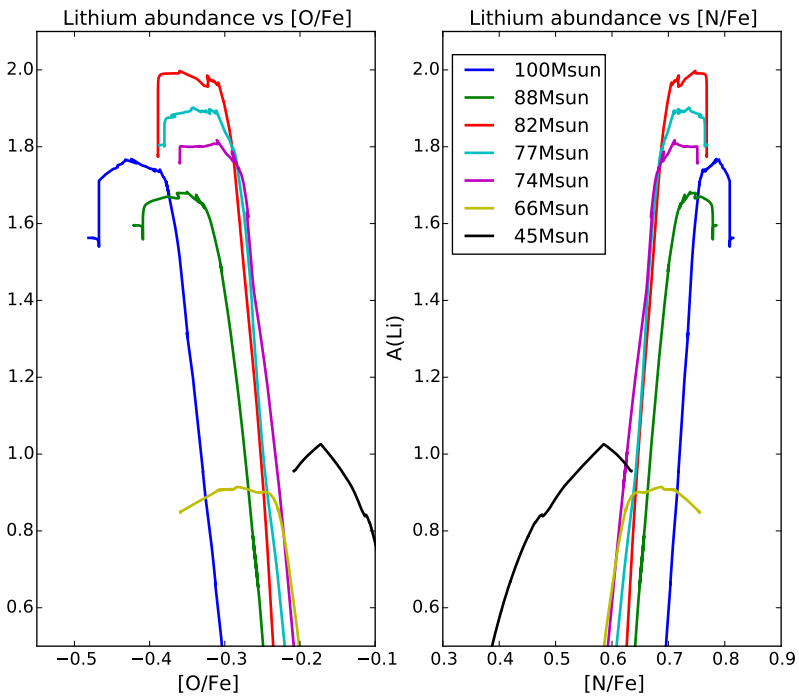


Figure 5: Lithium surface abundance vs oxygen and nitrogen at the surface of all models of differing mass. Zoomed to show the core helium burning phase where lithium levels are the highest in our models.

## 2.3 Lithium Production Mechanism

In the models created we see large amounts of lithium produced during the post main sequence phase of stellar evolution, that is, during the core helium burning and hydrogen shell burning phase. The mechanism for production relies specifically on the PPII chain and the role of convective envelopes adjacent to the hydrogen burning shell. The reaction in question, the PPII chain, can be shown simply as

$$^{7}_{3}\mathrm{Be} + e^{+} \rightarrow {}^{7}_{3}\mathrm{Li} + \nu_e \tag{3}$$

$$^{7}_{3}\mathrm{Li} + {}^{1}_{1}\mathrm{H} \rightarrow 2\,{}^{4}_{2}\mathrm{He} \tag{4}$$

The reaction of interest is the first one, in it a $^{7}$Be nucleus captures an electron and forms a $^{7}$Li nucleus. In most cases this lithium is quickly destroyed in the second reaction to form 2 $^{4}$He nuclei. In the our models, however, this lithium is removed from the hot region before it is destroyed. Kippenhahn diagrams are used to demonstrate this mechanism more explicitly.

### 2.3.1 Kippenhahn diagram for a 100 $M_{\odot}$ star

Figure 6 the Kippenhahn diagram for a star of initial mass $100M_{\odot}$ with metallicity $Z = 0.1 \times Z_{SMC}$ rotational velocity $v = 100kms^{-1}$.

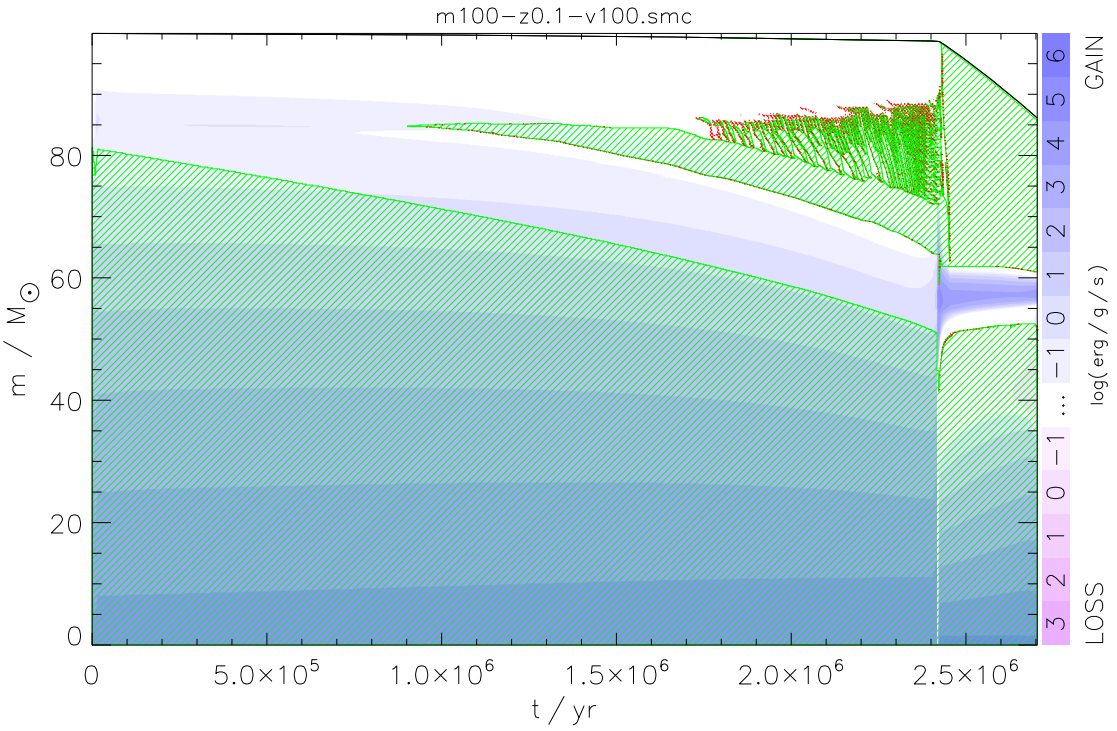


Figure 6: Kippenhahn diagram showing the evolution of qualitatively distinct layers in star with initial mass 100 $M_{\odot}$ over its lifetime. On the y-axis, mass is displayed (in solar units) and on the x-axis the time in years is shown. The pink and blue coloured scale is a key to the energy production/consumption and is indicative of nuclear burning with more blue/violet colours demonstrating high levels of energy production and pink hues endo-energetic processes i.e. neutrino flux. The green hatched lines show areas of convection in the star and red dots show areas of semi convection.

By looking at the green hatched areas of figure 6 we can see how the convective layers change over time. The initial convective envelope reaches up to $\sim 80 M_{\odot}$ of the star. Fusion occurs in a large portion of the star ($\sim 90 M_{\odot}$) as there is a small amount of energy production up to these layers. The inner convective layer decreases in size over time as the hydrogen fuel is consumed and fused into helium in turn decreasing the size of the fusion core. Near the end of the hydrogen core burning a convective envelope develops nearer the surface of the star and reaches further down as the star gets older. Semi convective areas form near the end of hydrogen core burning as well.

At around 2.4 Myr core hydrogen burning finished and core helium burning as well as hydrogen shell burning commences. The diagram shows two clear convective regions and an area of hydrogen shell burning in between these convective regions at around $\sim 60$ $M_{\odot}$. At this time there is also a large loss of material from this star compared to the main sequence with $\sim 15$ $M_{\odot}$ lost in the last few hundred thousands of years of the stellar model. This mass is lost as winds. The convective core is the area where further nuclear burning, or helium core burning, occurs.

At the same time the convective envelope reaches much deeper than at any other point in the stars evolution and also reaches the surface of the star. The blue/violet area in the diagram shows high levels of nuclear energy production indicating shell burning. As the convective envelope above reaches this area some lithium produced by the PPII chain in the hydrogen burning shell is mixed out of the burning region before it is destroyed. The final stage of stellar evolution is the period of scrutiny due to the high mass loss and high levels of lithium production.

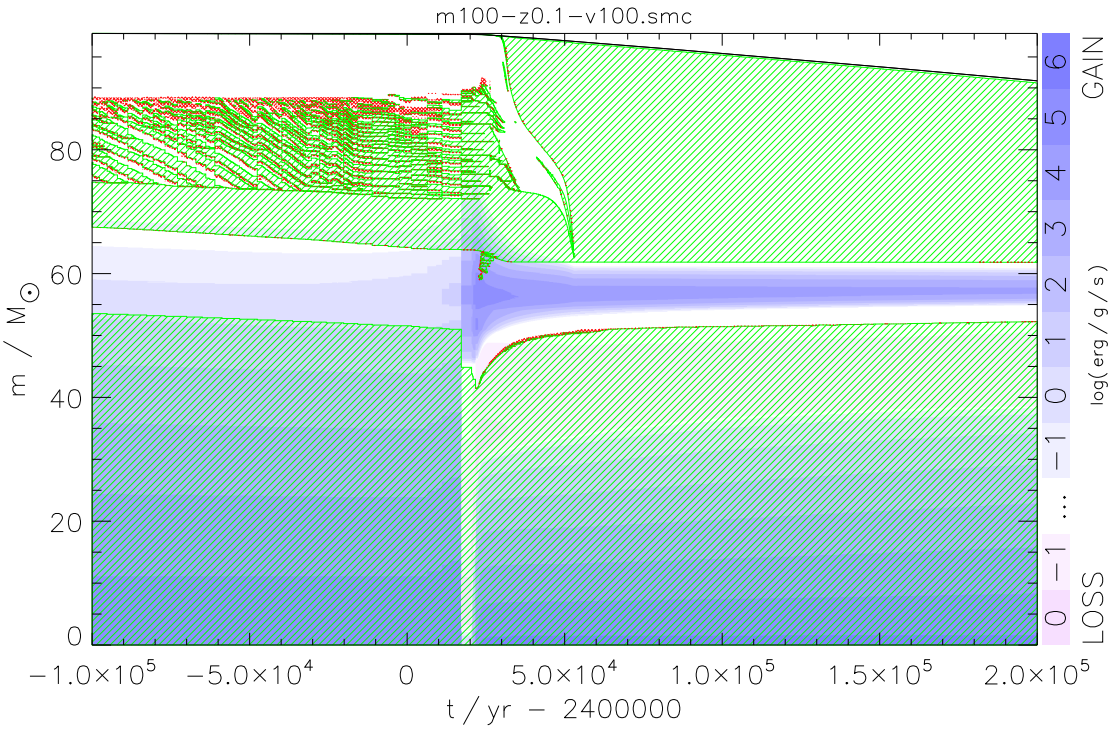


Figure 7: Kippenhahn diagram showing in more detail the hydrogen-burning shell of a star of initial mass 100 $M_{\odot}$ from Figure6, here we zoom into period around the end of the main-sequence.

At the core helium burning stage of the stars evolution the following features in the Kippenhahn diagram need to be considered. They are indicative of different physical processes. Starting in the middle of the star i.e. bottom of the diagram, large amounts of nuclear energy production is seen. This is due to helium burning, with the core extending almost halfway up the star. The highest amount of burning occurs in the middle of the star as the temperature in this area is highest meaning more helium can fuse more often via the triple alpha process. Further up in the convective core energy production can be seen to end and energy loss occurs, due mainly to a flux of neutrinos. In between the two convective zones is a region of high nuclear energy production i.e. hydrogen shell burning. This burning shell is not hot enough for the CNO cycle to dominate, meaning the PP chains dominate here. As discussed previously in section 1.2.1, in most stars the lithium formed by the PPII chain will quickly fuse with another hydrogen nucleus to form 2 $^4$He nuclei. If, however, there is a convective envelope that reaches down to this hydrogen burning shell then the lithium can be transferred to the cooler convective envelope above, thus preserving the delicate lithium nucleus. The convective envelope only overlaps the hydrogen burning shell for a small period starting at $\sim 2.42\ Myr$ and finally ending $\sim 2.45\ Myr$. This coincides with the high rate of lithium production seen in the surface plots. Although the convective shell does not reach the surface at the time when there is an overlap, the lithium can be retained in the cooler areas of the envelope until it reaches the surface at around the time the overlap ends. When this convective shell reaches the surface it allows much of the lithium rich material to be ejected as winds. The relatively high amount of mass loss at this phase leads to a significant amount of lithium to be lost as winds. According to the diagram approximately $\sim 15\ M_{\odot}$ of material is lost in the helium core burning phase which lasts for $\sim 0.25\ Myr$.

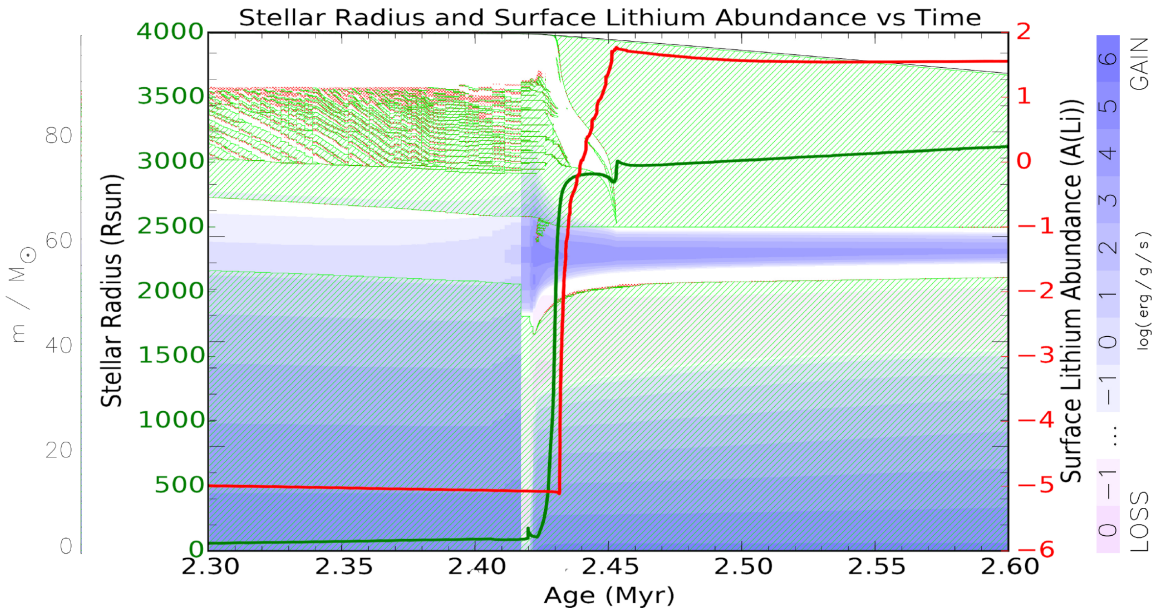


Figure 8: Kippenhahn diagram showing in more detail the hydrogen shell-burning phase of stellar evolution of a star of initial mass 100 $M_{\odot}$ with the lithium surface abundance and radius in solar units overlayed.

### 2.3.2 Varying Initial Mass

To study the mechanism of lithium production and its effects in more detail, we have computed 7 new models with varying mass and rotational velocities. We used the same initial composition as in Szécsi et al (2015), as this is representative for most globular clusters (see fig. 2 in Szécsi et al (2017)). The models of initial mass $45, 77$ and 100 $M_{\odot}$ were taken from Szécsi et al (2015), while all other models presented in this work were computed by us. Models of mass 66 $M_{\odot}$, 74 $M_{\odot}$, 82 $M_{\odot}$ and 88 $M_{\odot}$ were computed. These masses were chosen to be close to model the largest lithium production, this was the model with initial mass 77 $M_{\odot}$. Surface abundance over time is displayed for all models in Figure. 9.

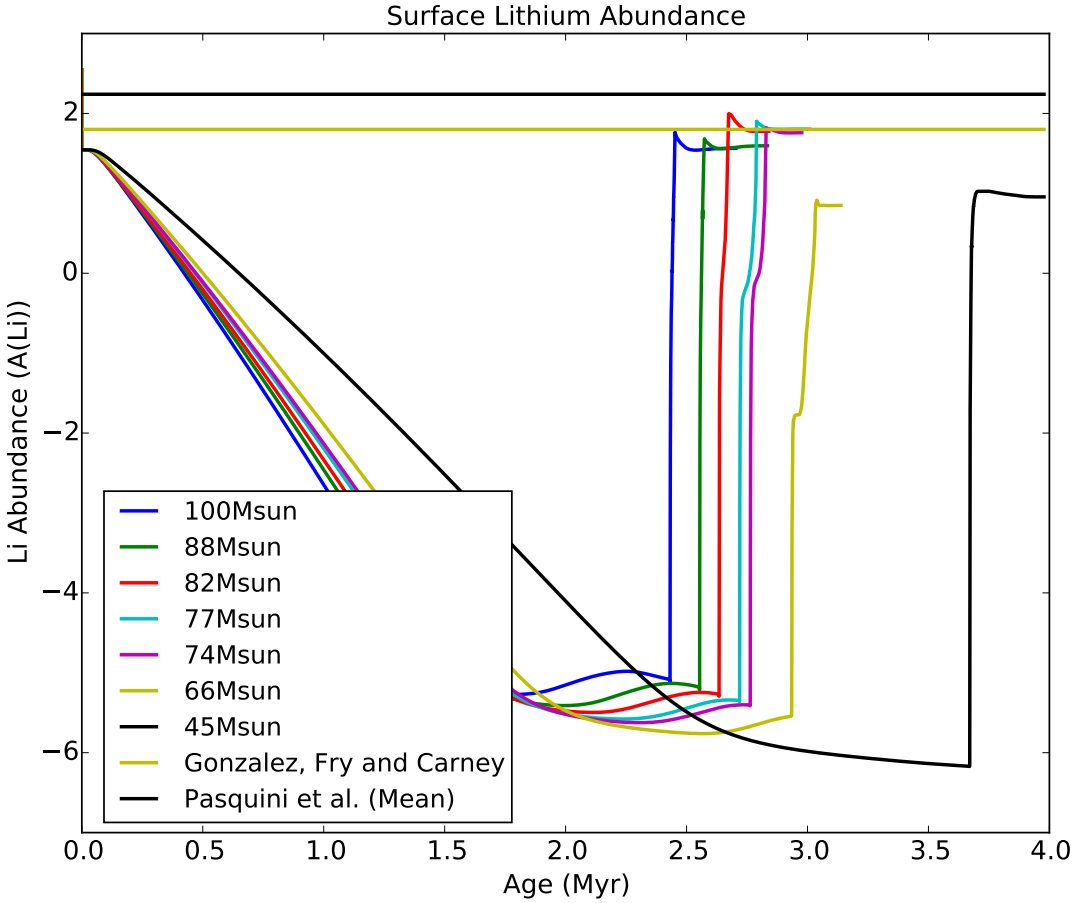


Figure 9: Lithium surface abundance levels for 7 stellar models. Reference abundances are displayed, these were taken from observations of lithium abundance in some GC stars. Carney, Fry and Gonzalez (1998(@) calculated levels are shown along with the mean Pasquini et al (2005) observations.

Figure 9 shows that the 82 $M_{\odot}$ model exhibits the largest amount of lithium production with other models closer to 100 $M_{\odot}$ showing higher levels of lithium production compared to models closer to 45 $M_{\odot}$. The reason for the spread of lithium production for different masses is thought to be that some models experience a longer overlap of the convective envelope and the hydrogen burning shell, saving more lithium from destruction. Future work is required however to explain the physical reason for this variation in overlap length.

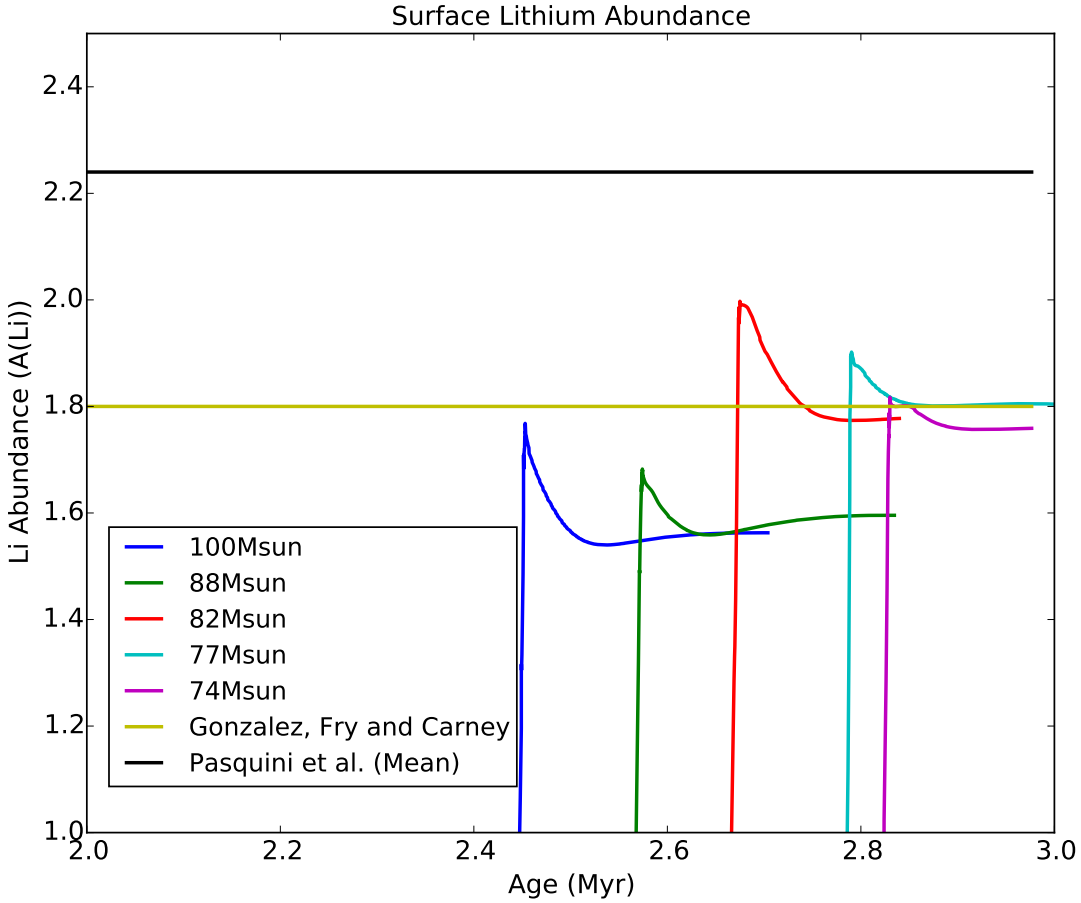


Figure 10: Lithium surface abundance levels for 5 of the most lithium productive stellar models, zoomed to show more detail at the lithium production stage. Reference abundances are displayed, these were taken from observations of lithium abundance in some GC stars. Carney, Fry and Gonzalez (1998(@) calculated levels are shown along with the mean Pasquini et al (2005) observations.

### 2.3.3 Varying Initial Rotational Velocity

Rotational velocity was another parameter which we looked at closely, with a number of new models created with initial mass 77 $M_{\odot}$. Szécsi et al (2015) have shown that stars with high rotational velocities of $\geq$ 200 $kms^{-1}$ can start to undergo chemically homogeneous evolution. This process affects the formation of the convective envelope of our massive stars and so will in turn cancel out the lithium production mechanism. When it came to lower rotational velocities we could also infer that rotation, while much smaller compared to just convectional mixing, still had an impact on the levels of lithium produced. With this in mind models were produced using an initial mass of 77 $M_{\odot}$, with the rotational velocity varied by $\pm$25 $kms^{-1}$ compared to the original model, i.e 75 and 125$kms^{-1}$. A further model was created for a 77 $M_{\odot}$ star and 50 $kms^{-1}$.

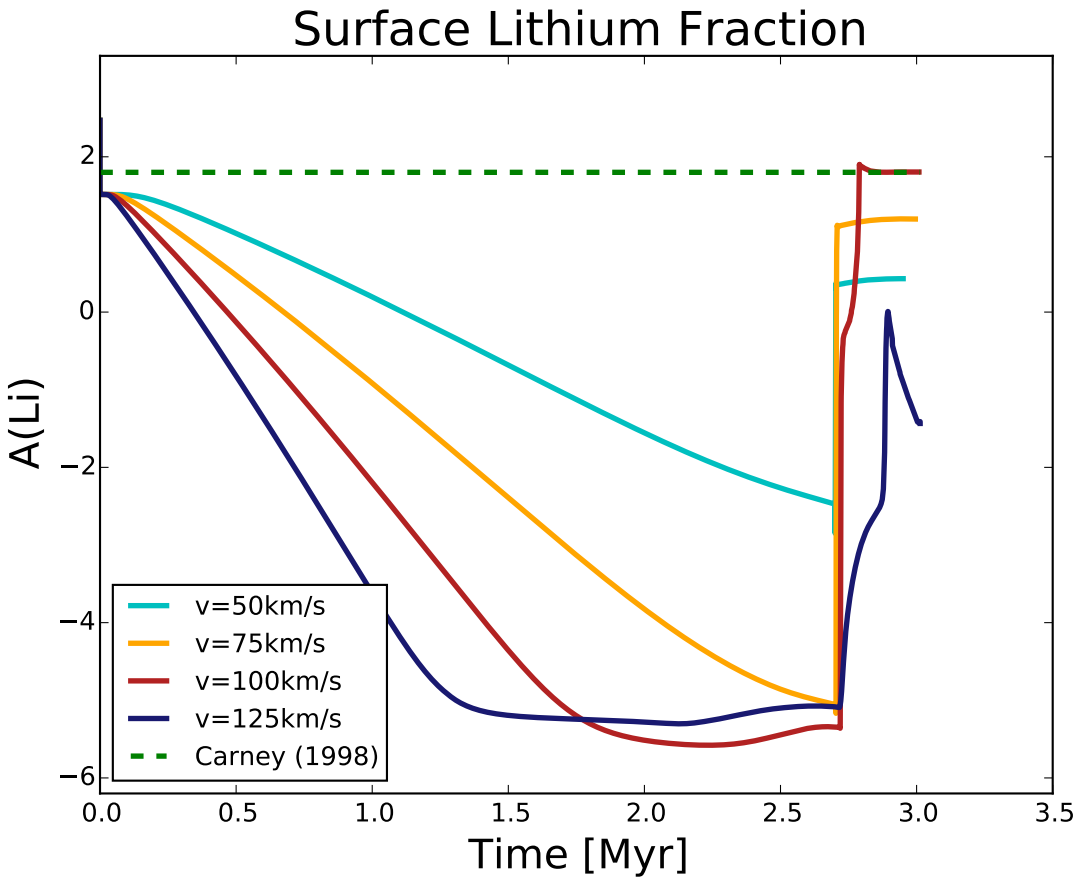


Figure 11: Lithium surface abundance levels for 4 stellar models of varying mass and rotational velocities. Fry, Carney and Gonzalez calculated levels are shown along with the mean Pasquini at al 2005 observations.

The lithium abundance at the surface is found to depend strongly on the rotational velocity. Lower rotational velocity results in less lithium depletion during the main sequence as the rotational mixing is not as efficient at bringing the surface lithium deeper into the star where it would be destroyed. The light blue line in Figure 11 which corresponds to model with the lowest rotational velocity ($50 kms^{-1}$) shows significantly less lithium depletion during the main sequence, this is due to the surface temperatures not exceeding the lithium burning temperature as well as the decreased rotational mixing reducing the efficiency of the mixing as a whole. Although the lithium depletion during the main sequence is diminished, this does not affect the lithium production in the post main sequence since the production mechanism is more or less independent from rotational mixing, Lower rotational mixing in the post main sequence also acts to reduce the efficiency of the lithium production mechanism. The models show the largest levels of lithium production for an initial rotational velocity of $v = 100 kms^{-1}$.

The model with $v = 125 kms^{-1}$ shows some lithium production during the post main sequence. However rotational mixing in this model means that the lithium, once produced, may be mixed back into the interior of the star where is is destroyed leading to a less efficient lithium production mechanism. Another feature in the lithium surface abundance plot for this model is the rapid depletion of lithium after it has been produced in during the post main sequence. This is due to more rotational mixing during the main sequence leading to a higher surface helium abundance, figures demonstrating this can be found in section A.6, this in turn reduces the opacity leading to a higher surface temperature. Lithium present in the surface would then be rapidly destroyed.

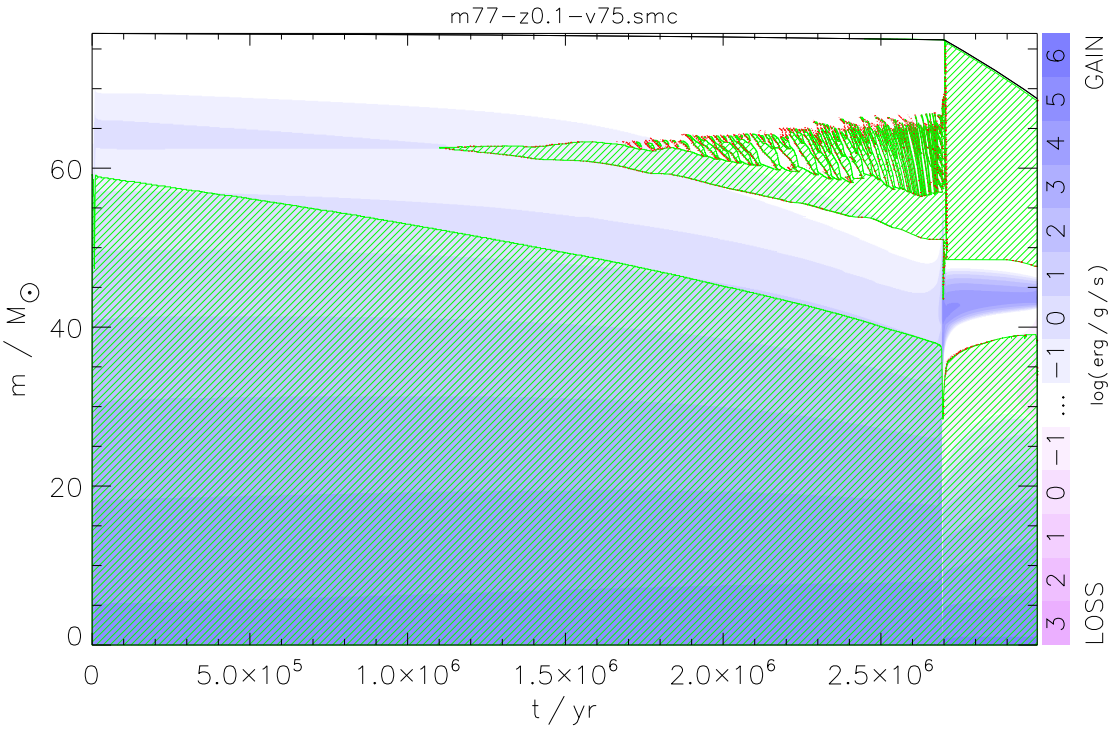


Figure 12: Kippenhahn diagram showing the stellar evolution of a star of initial mass 77 $M_{\odot}$ and rotational velocity $75 kms^{-1}$.

## 2.4 Dispersion mechanism

We have a mechanism for lithium production and carefully constrained the relevant parameters that would lead to higher lithium production. Now we require a mechanism that could successfully distribute most, if not all, of the material in these models such that they could be used to explain observations of certain stars in globular clusters. To explain observed abundances a mechanism is required that could successfully incorporate the stellar material into the intra-cluster medium (ICM) in a young globular cluster. The models show significant mass loss due to winds during the core helium burning phase. However, a large portion of the lithium is still present in the star at the end of this phase. If we required 100% efficiency of dispersion, other pathways are discussed in section 2.4.5 and 2.4.6.

### 2.4.1 Winds

Low metallicity massive stars suffer a significantly lower amount of mass loss as winds than high metallicity stars during the main sequence. We discuss here the amount of lithium that can be expelled as winds during the post main sequence after lithium has been produced. With a high lithium abundance in the surface, the next step is to calculate the amount of lithium present in the entire star as well as the amount ejected as winds, specifically during the post main sequence. The amount of lithium shown in Table 2.4.4, each stellar model is show as well as the mass of lithium present at the end of the post main sequence/ helium core burning phase. This was to give an indication as to the theoretical maximum amount of lithium that could be ejected or accreted from the star at the end its evolution. The mass of lithium ejected as winds was also calculated for all the models. This gave a further indication of the amount lithium that had been dispersed. the figure shown below shows the mass of lithium in the star as a function of time.

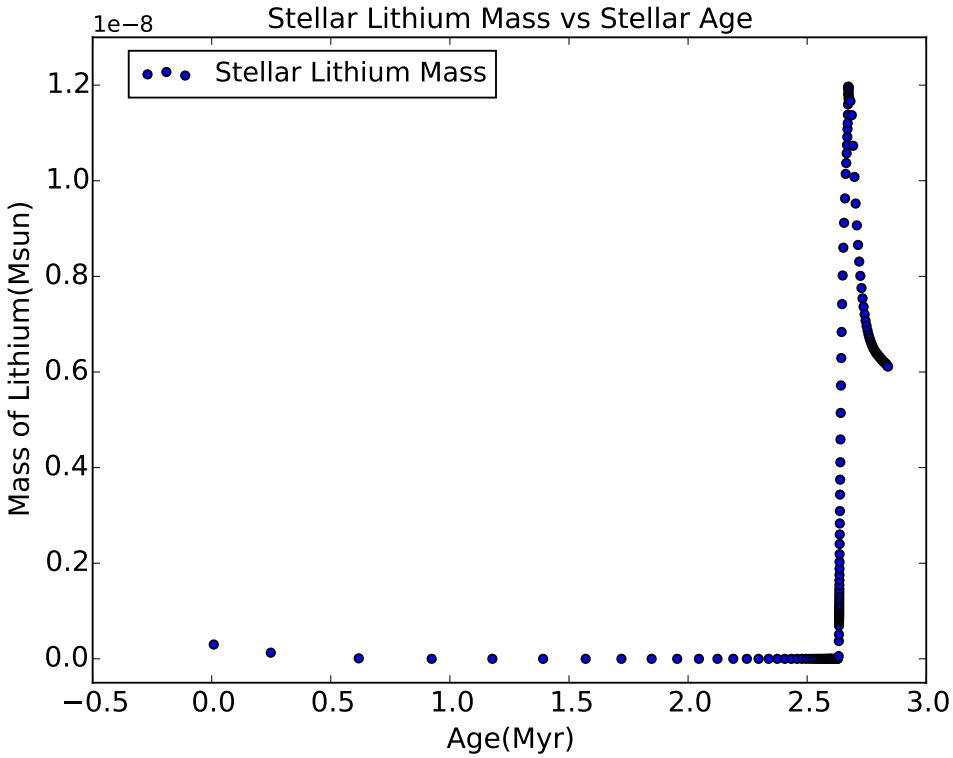


Figure 13: Mass of lithium in entire star for a stellar model of initial mass 82 $M_{\odot}$.

### 2.4.2 Lithium levels in clusters

By using the output of the models we were able to calculate the amount of lithium produced by each star as well as the lithium lost as winds in each model. For this calculation we integrated up the whole star from core to surface to determine the mass of lithium present. For the winds we summed over the amount of lithium at the surface, weighting with the mass loss rate over time, as the lithium itself resided in the surface.

### 2.4.3 The IMF

Considering a typical initial mass function (IMF) derived by (Salpeter , 1995), we get an order of magnitude estimate for the lithium produced in a typical cluster. Given that we could estimate the total lithium mass produced by each model, we predict the number of stars of each mass in a given mass in a cluster of mass $10^6 M_{\odot}$. We assume linearity when interpolating between the initial masses and that no lithium is produced by stars with initial mass outside the range $45 - 100\ M_{\odot}$. We assume that all mass in the cluster is used to form stars, and indeed into first generation stars. This is a simplistic assumption as we know that most of the mass in the Universe is not trapped in stars. We also assume that all mass is conserved in the cluster, which again may be unlikely given that winds and supernovae could provide mechanisms for gas ejection from a young cluster. We do not consider a rotational velocity distribution in this estimate and so assume that all stars have a rotational velocity of 100 $kms^{-1}$ though future work could used distributions such as those described in Mokiem et al (2006). The IMF used for this estimate was the Kroupa (2001)/Salpeter (1995) distribution shown in more detail in section A.2. Although some researchers suggest that some of the first structures to form from the primordial gas could have had an IMF that favoured higher mass stars, and this suggestion would be better for our case as it would result in a higher lithium estimate, it was only realistic to use the IMF that has been studied in more detail.

### 2.4.4 Typical cluster estimates

Our estimates for the maximum lithium produced in a $10^6 M_{\odot}$ used the 7 models of varying mass and a constant initial rotational velocity of $100 kms^{-1}$. The table shown details the lithium lost in winds along with the total lithium still present in the star at the end of evolution. The sum of these values is also shown with these being the values used in our cluster estimate in the total lithium produced column.

| Lithium production in models | | | |
|---|---|---|---|
| Model initial mass ($M_{\odot}$) | Lithium lost as winds ($M_{\odot}$) | Lithium remaining in star ($M_{\odot}$) | Total Lithium produced ($M_{\odot}$) |
| 45 | $7.12 \times 10^{-10}$ | $7.27 \times 10^{-11}$ | $7.85 \times 10^{-10}$ |
| 66 | $6.67 \times 10^{-10}$ | $6.81 \times 10^{-11}$ | $7.35 \times 10^{-10}$ |
| 74 | $5.62 \times 10^{-9}$ | $8.32 \times 10^{-10}$ | $6.45 \times 10^{-9}$ |
| 77 | $5.84 \times 10^{-9}$ | $1.46 \times 10^{-9}$ | $7.3 \times 10^{-9}$ |
| 82 | $6.11 \times 10^{-9}$ | $1.36 \times 10^{-9}$ | $7.47 \times 10^{-9}$ |
| 88 | $3.75 \times 10^{-9}$ | $1.42 \times 10^{-9}$ | $5.17 \times 10^{-9}$ |
| 100 | $3.42 \times 10^{-9}$ | $1.66 \times 10^{-9}$ | $5.08 \times 10^{-9}$ |

An observation from these results is that the mass of lithium lost as winds is an order of magnitude less than is left in the star at the end of its life in the lower mass stars however as mass increases and indeed mass loss increases a significant fraction of lithium in the star is lost as winds. From these results we calculated that $\sim 10^{-6}$ $M_{\odot}$ of lithium was produced in total (including winds) by a $10^6$ $M_{\odot}$ cluster, and one order of magnitude less ($\sim 10^{-7}$ $M_{\odot}$) lithium ejected as winds only. We also estimate the number of stars that could form from this material and have an abundance of $A(Li) = 2$. Our calculations put this figure at $\sim 10^3$ solar mass stars.

### 2.4.5 Binary Stripping

A mechanism which is able to disperse the entire lithium containing envelope is the scenario called binary stripping discussed in section 1.6. Given that the majority of massive stars have binary companions and can have binary interactions in their lifetime, it was reasonable to investigate a scenario whereby a binary companion strips the entire envelope once the lithium had been produced. We investigated the exact timing of the lithium production in these stars as well as when the lithium was at its maximum levels and compared this to the radius of star. Case B binary stripping occurs when the donor is evolving to the supergiant phase. We expect that the most likely period when a star undergoes binary mass transfer is during this evolution to a red supergiant, as the radius increases by $\sim 2$ orders of magnitude. In this period the star can overflow its Roche lobe and transfer mass onto the accretor. Figure 14 demonstrates that the lithium is not created until the radius of the stars increases significantly. This may mean that many of our models will be stripped before the lithium is created. It does not, however, completely rule out the possibility of an effective stripping but may require fine tuning of the separation distance of the companion. In any case, further work is required here.

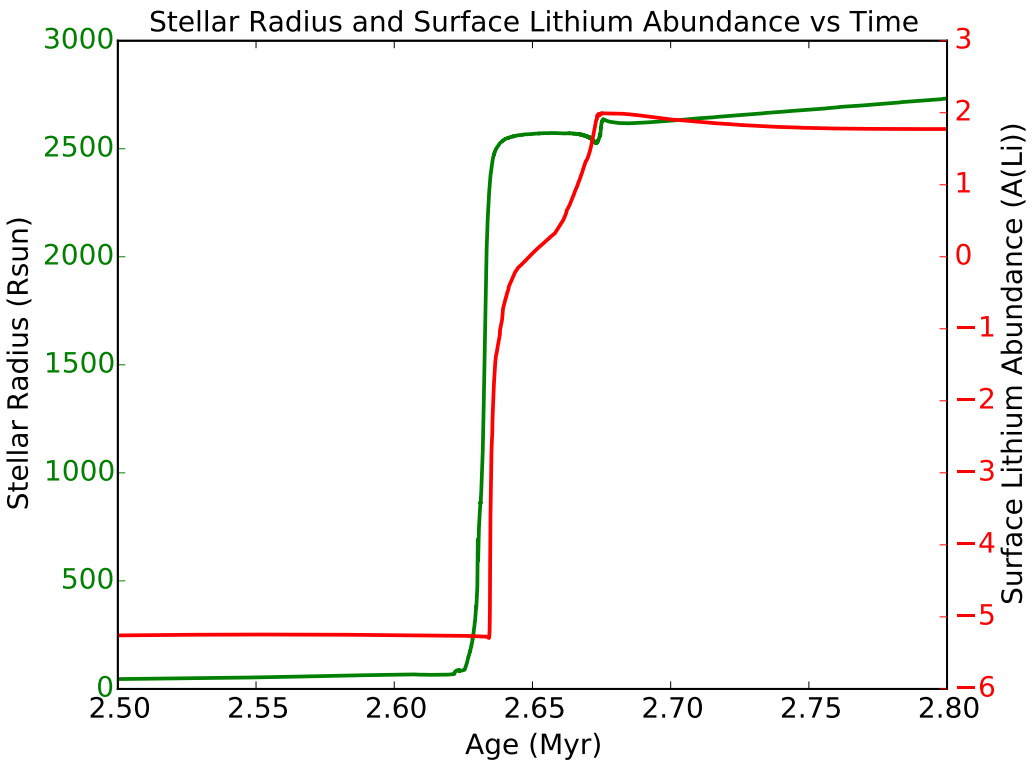


Figure 14: Lithium production (A(Li)) in red and Radius of star in solar units in green versus time, zoomed in to the start of core helium burning for a star of initial mass 82 $M_{\odot}$.

### 2.4.6 Other Mechanisms

Apart from the binary stripping mode of ejection from the system, a common envelope phase involving a binary companion could be of interest. This may provide an ejection mechanism and give the stars the time to produce the lithium. Another mechanism, proposed by Szécsi et al (2017) could also be promising in accounting for the dispersion of the lithium. The mechanism involves the trapping of supergiant winds in shells by the ionising radiation of neighbouring stars. While the stars investigated were more massive that our models ($120 - 600$ $M_{\odot}$) the possibility of this mechanism to apply to stars of mass $\sim 80$ $M_{\odot}$ is suggested. This mechanism allows low mass stars to form from the ejected material only meaning they will exhibit the same composition as the supergiant winds.

# 3 Conclusion and Discussion

We have used the Binary Evolution Code (BEC) to produce single stars models from zero age main sequence to the end of core helium burning. These stars had initial masses that ranged from 45 $M_{\odot}$ to 100 $M_{\odot}$ and initial surface rotational velocities that ranged from 50 $kms^{-1}$ to 125 $kms^{-1}$. All stars modelled had a metallicity of 0.1 times that of the Small Magallenic Cloud or 1/50th solar metallicity. All models showed large amounts of lithium produced at the beginning of core helium burning. The mechanism responsible for lithium production was investigated and it was found that it was due to a convective envelope reaching into a hydrogen burning shell which through the PPII chain formed $^{7}$Li which could be removed before it was destroyed. The effect of mass and rotational velocity was investigated on the efficiency of this process. The models that produced the most lithium had initial masses around 80 $M_{\odot}$ and initial rotational velocities of 100 $kms^{-1}$. The model that produced the most lithium had a mass of 82 $M_{\odot}$. High rotational velocity revealed a modest level of lithium production, however the lithium present in the surface was rapidly depleted after it was produced. A mechanism which could disperse the lithium from the models was also investigated. This mechanism would ideally be able to account for the observed abnormalities in lithium abundance in some stars in globular clusters. We considered that winds would be the first channel of inquiry as all models exhibited high mass loss during the post main sequence when the lithium was at its highest abundance. This wind would also be lithium rich as the material ejected from the star was from the surface. An order of mass calculation was carried out which gave an estimate as to the amount of lithium that could possibly be produced in a cluster of a typical mass $10^{6}$ $M_{\odot}$. We found that the total mass produced was of order $10^{-6}$ $M_{\odot}$ and that expelled by winds was of order $10^{-7}$ $M_{\odot}$. We speculated about a binary stripping event: while it remains a possible mechanism, the radius change would make it more likely that a star of these sizes would be stripped before lithium has been produced. The dynamics of globular clusters and the details of their star formation is a rapidly developing field in the present day. The purpose of this investigation was to give more insight to the evolution of globular clusters, however, it is clear much more is needed to ensure an accurate picture is obtained.

## 3.1 Outlook

We have presented a promising mechanism for lithium production in massive low metallicity stars. Whether this mechanism accounts for most of the lithium present in GCs, or indeed any of it, needs more investigation. More work is also required on the dispersion of the new lithium. The production of binary models is a rational next step, with a common envelope phase presenting an opportunity for further research. The lithium production mechanism itself was qualitatively explained. A more detailed analysis of this process can not only help to give a more complete picture of stellar evolution but may help in explaining the distribution of lithium in the Universe. More models should be created to give a statistically significant hypothesis of relevant anti-correlations observed in globular clusters.

# 4 Acknowledgements

I would like to thank Dr. Dorottya Szécsi in particular for her continued help, not only with the project but inspiring me to get the most out of myself. Her knowledge on the subject was both useful and interesting, giving me fascinating insight into stellar evolution and the dynamics of globular clusters. I would also like to thank Prof. Ilya Mandel for his incredible knowledge on many subjects pertaining to the project, in particular his help regarding binary systems. My project partner Sam Ratcliff also deserves credit for his help regarding particularly challenging problems we faced.

## Bibliography

Bastian, N., Lamers, H. J. G. L. M., de Mink, S. E., et al 2013, arXiv:1309.3566v1

Carney, B. W., Fry, A. M., Gonzalez, G., 1998, The Astronomical Journal 116, 2984-2992

Carretta, E., Bragaglia, A., Gratton, R., et al 2009, A&A, 505, 117-138

Carretta, E., Bragaglia, A., Gratton, R., et al 2010, arXiv:1002.0002v1

Chandrasekhar, S.,1931, ApJ, 74, 81-82

Crowther, P. A., Schnurr, O., Hirschi, R., et al 2010, Mon. Not. Astron. Soc., arXiv:1007.3284v1

D'Orazi, V., Gratton, R. G., Angelou, G.C. et al 2015, Mon. Not. Astron. Soc., arXiv:1503.05925v1

Figer, D. F.,2005, Nature, 434, 192-194

Gratton, R. G., Carretta, E., Bragaglia, A., 2012, arXiv:1201.6526v1

Kasen, D., Metzger, B., Barnes, J., et al 2017, Nature 551, 80-84

Krauss, L. M., Chaboyer, B. 2003, Science, 299, 65-69

Kroupa, P.,2001, arXiv:astro-ph/0009005

Lada, C. J., 2009, arXiv:0911.0779

Larsen, S. S., Brodie, J. P., Forbes, D. A. et al 2014, A&A, 565, A98

Matteucci, F., Romano, D., 2000, IAUS, 198, 558M

Mokiem, M. R., de Koter A., Evans, C. J., et al 2006, A&A, arXiv:astro-ph/0606403v1

Monaco, L., Villanova, S., Bonifacio, P., et al 2012, A&A, 539, A157

Oberhummer, H., Pichler, R., Csótó, A.,1999, arXiv:nucl-th/9810057v2

Pasquini, L., Bonifacio, P., Molaro, P., et al 2005, A&A, 441, 549-553

Pelupessy, F. I. and Zwart, S. P. 2011, arXiv:1111.0992v1

Piotto, G., Bedin, L. R., Anderson, J., et al 2007, ApJ, 661, L53-L56

Piotto, G., Milone, A. P., Anderson, J., et al 2012, ApJ, 760, 39

Puls, J., Vink, S. J., Najarro, F.,2008, A&AR, 16, 209-325

Ray, A. arXiv: 0907.5407v1

Salpeter, E. E., 1995, ApJ 121

Stothers, R. B., Chin, C-W.,1995, ApJ, 451, 61-64

Szécsi, D., Langer, N., Yoon, S-C., et al, 2015, A&A 581, A15

Szécsi, D., Makey, J., Langer, N., 2017, A&A, arXiv:1711.04007v1

Villanova, S., Piotto, G., King, I. R., et al 2007, ApJ, 663, 296-314

Villante, F.L., Dolgov, A.D.,2003, hep-ph/0310138, 2

# A Appendix

## A.1 Elemental abundance units

In this paper we have used particular abundance units for elements in our models. Although we are able to produce absolute values in our models of certain elements, in order to usefully compare the abundances to observations we must use observational units. This entails presenting elemental abundances as fractional abundances of Hydrogen (H) and Iron (Fe). With the lithium abundances observers compare spectral lines for lithium and hydrogen and use solar values as a calibration.

For the lithium abundance values, A(Li) was used as it is the unit used in astronomical observations including the observations which were relied upon. To determine A(Li) the following equations were used.

$$A(Li) = [Li/H] = log_{10}\left(\frac{Li}{Li_{\odot}}\right) - log_{10}\left(\frac{H}{H_{\odot}}\right) \tag{5}$$

Similarly for the other elemental abundances the following equations were used. Here $X$ represents the element of interest.

$$[X/Fe] = log_{10}\left(\frac{X}{Fe}\right) - log_{10}\left(\frac{X}{Fe}\right)_{\odot} \tag{6}$$

$$[X/Fe] = \left[log_{10}\left(\frac{X}{H}\right) - log_{10}\left(\frac{X}{H}\right)_{\odot}\right] - \left[log_{10}\left(\frac{Fe}{H}\right) - log_{10}\left(\frac{Fe}{H}\right)_{\odot}\right] \tag{7}$$

## A.2 The IMF

The Salpeter 1955/ Kroupa 2001 IMF used for the estimates in section (SECTION REF) relied upon a distribution described mathematically as

$$\xi(m) \propto m^{-\alpha_i} = m^{\gamma_i} \tag{8}$$

where

$$a_0 = +0.3 \pm 0.7,\ 0.01 \leqslant \frac{m}{M_{\odot}} < 0.08 \tag{9}$$

$$a_1 = +1.3 \pm 0.5,\ 0.08 \leqslant \frac{m}{M_{\odot}} < 0.50 \tag{10}$$

$$a_2 = +2.3 \pm 0.3,\ 0.5 \leqslant \frac{m}{M_{\odot}} < 1.00 \tag{11}$$

$$a_3 = +2.3 \pm 0.7,\ 1.00 \leqslant \frac{m}{M_{\odot}} \tag{12}$$

as we are only concerned with stars of mass $> 1.00M_{\odot}$ we need only consider the exponent in equation 12.

## A.3 Binary Evolution Code

The binary evolution code or BEC is able to produce 1 dimensional hydrodynamical simulations of single and binary stars. The code can account for rotation, mass-loss and the transport of angular momentum. The code outputs a large number of data sets, including elemental abundances, mass, temperature, convection and nuclear burning.

## A.4 Kippenhahn Diagrams

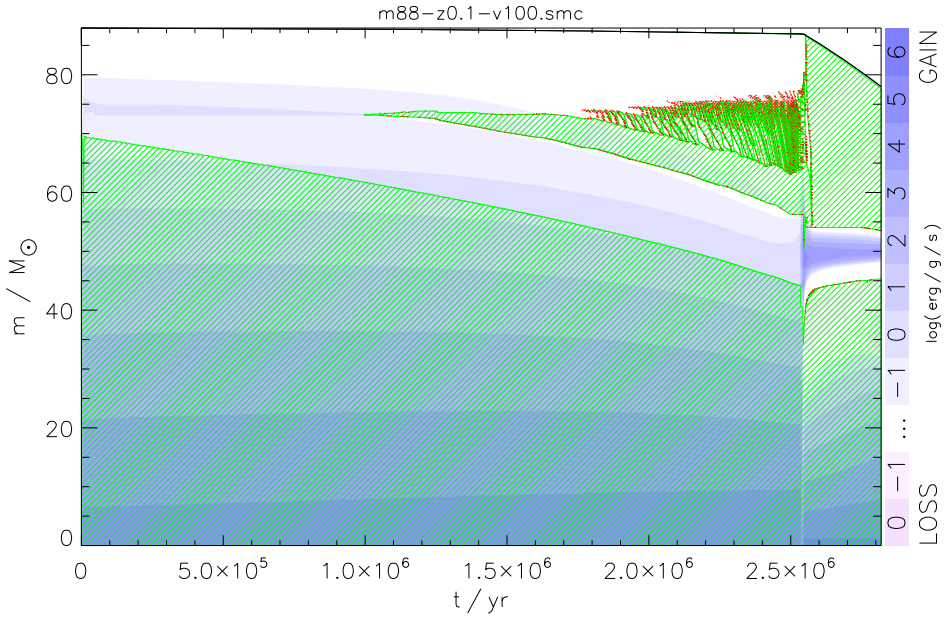


Figure 15: Kippenhahn diagram showing the stellar evolution of a star of initial mass 88 $M_{\odot}$.

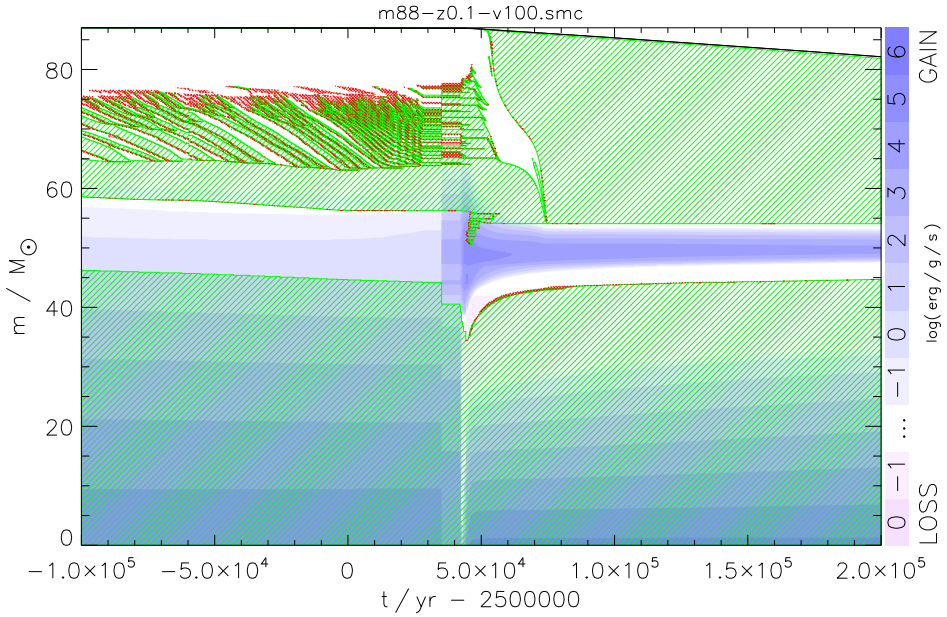


Figure 16: Kippenhahn diagram showing the stellar evolution of a star of initial mass 88 $M_{\odot}$ zoomed to show the end of the core hydrogen burning and the beginning of the core helium burning.

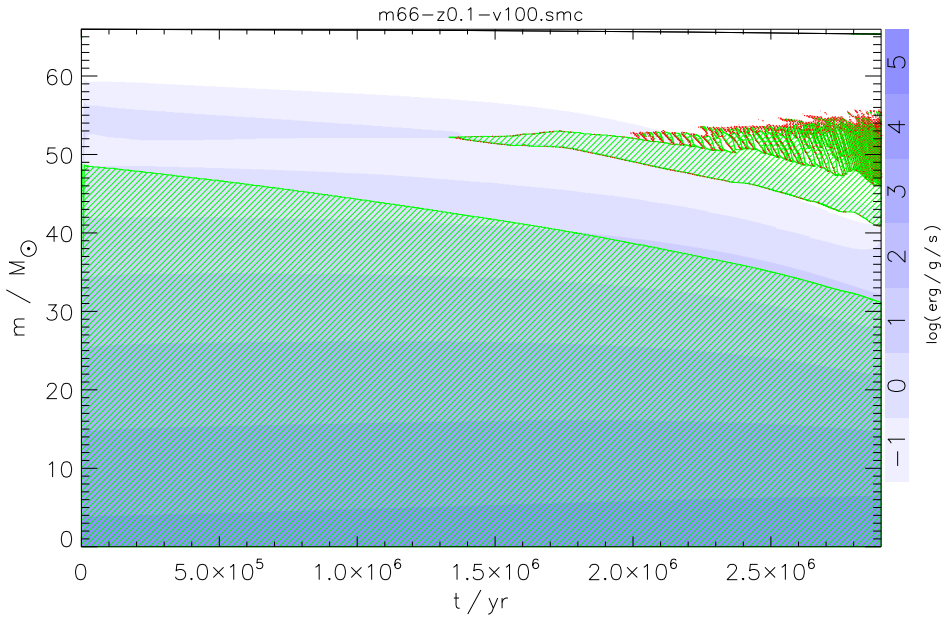


Figure 17: Kippenhahn diagram showing the stellar evolution of a star of initial mass 66 $M_{\odot}$.

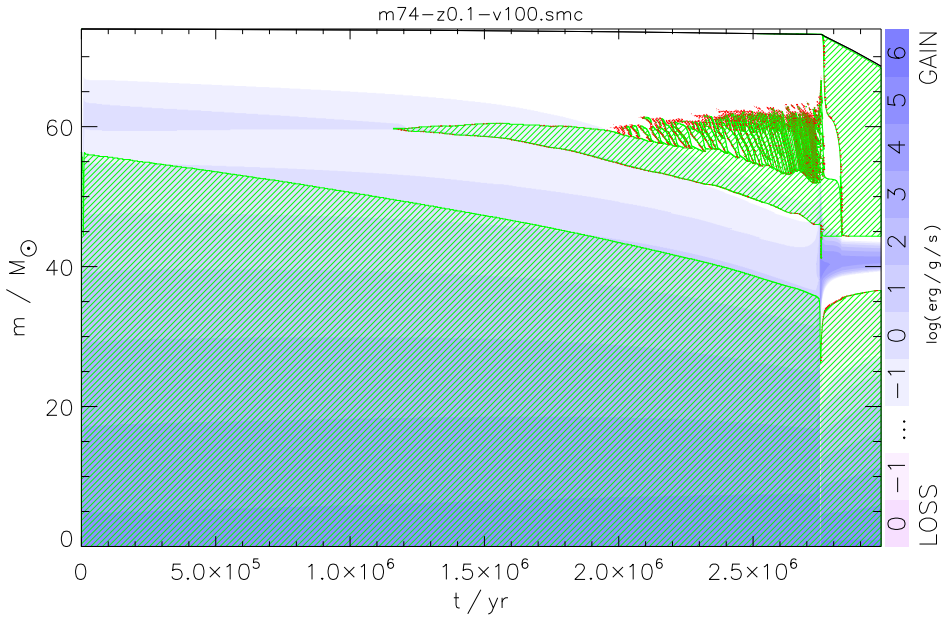


Figure 18: Kippenhahn diagram showing the stellar evolution of a star of initial mass 74 $M_{\odot}$.

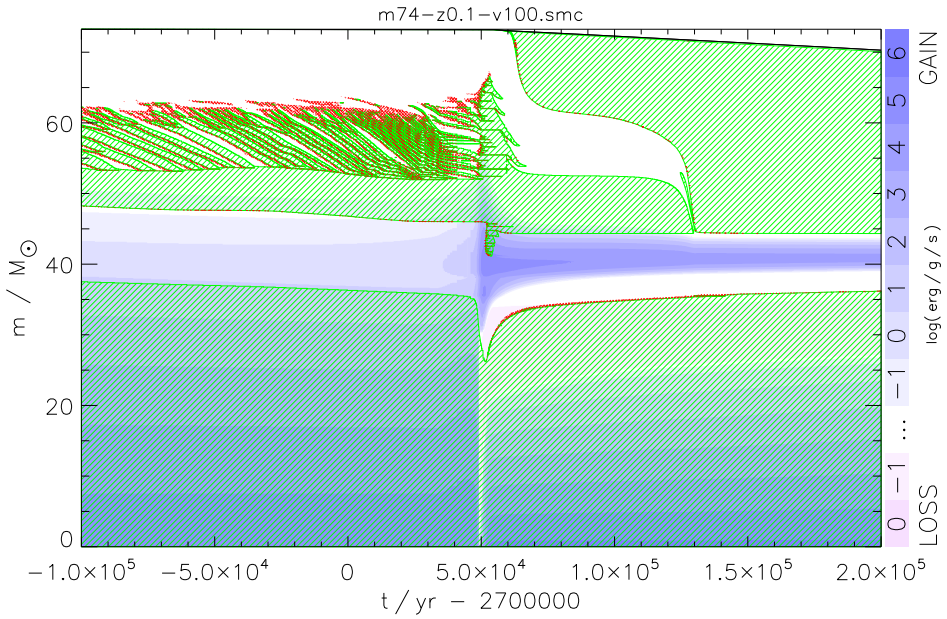


Figure 19: Kippenhahn diagram showing the stellar evolution of a star of initial mass 74 $M_{\odot}$.

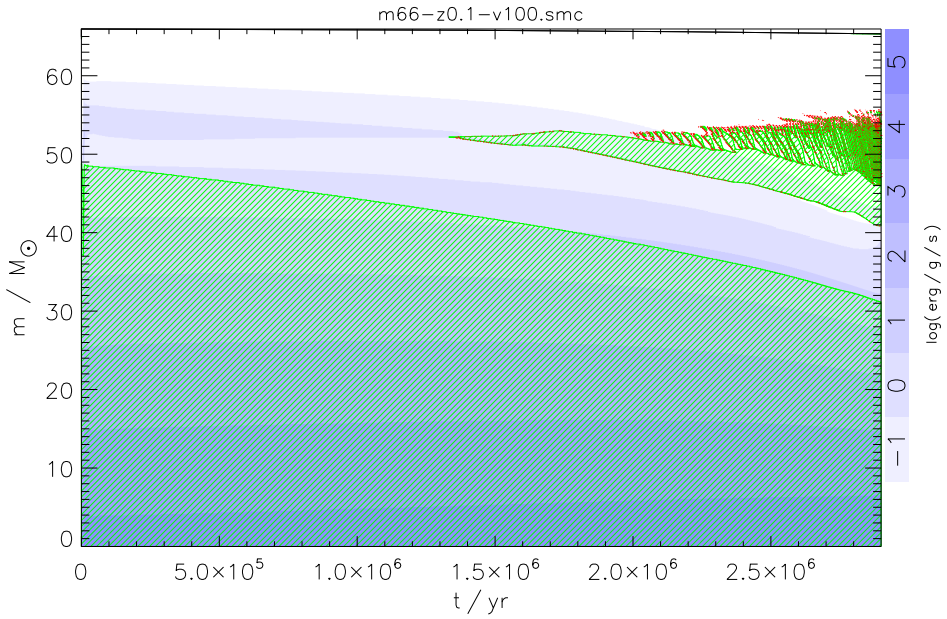


Figure 20: Kippenhahn diagram showing the stellar evolution of a star of initial mass 66 $M_{\odot}$.

## A.5 Radius/Surface Lithium Plots

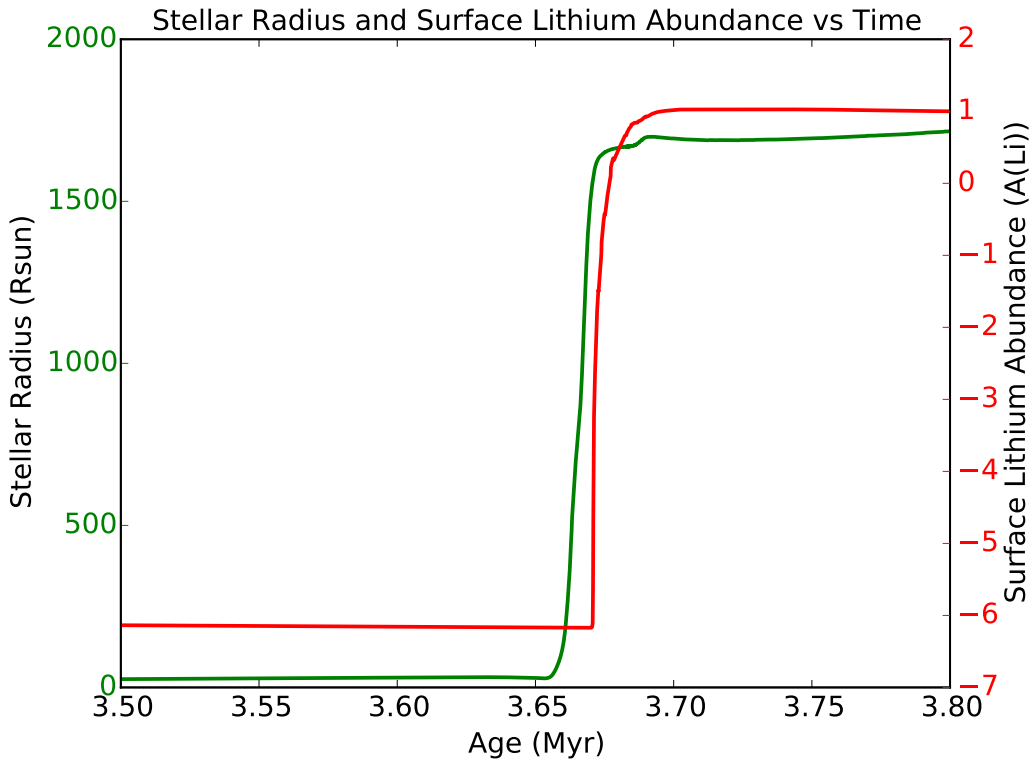


Figure 21: Lithium production (A(Li)) in red and Radius of star in solar units in green versus time, zoomed in to the start of core helium burning for a star of initial mass 45 $M_{\odot}$.

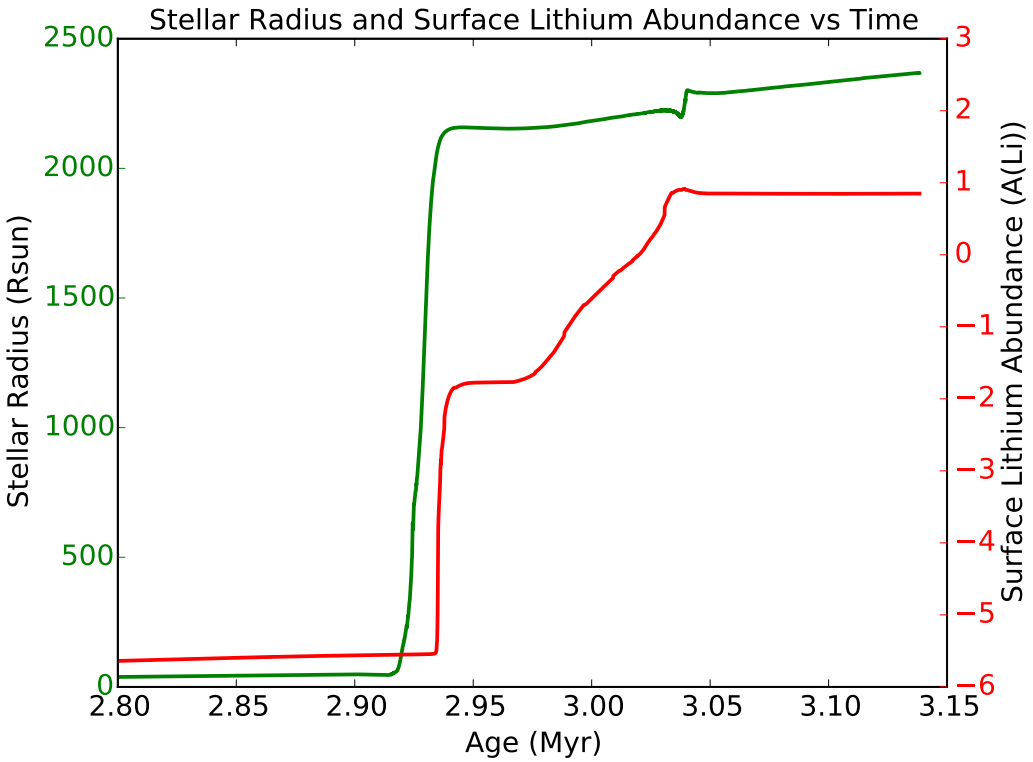


Figure 22: Lithium production (A(Li)) in red and Radius of star in solar units in green versus time, zoomed in to the start of core helium burning for a star of initial mass 66 $M_{\odot}$.

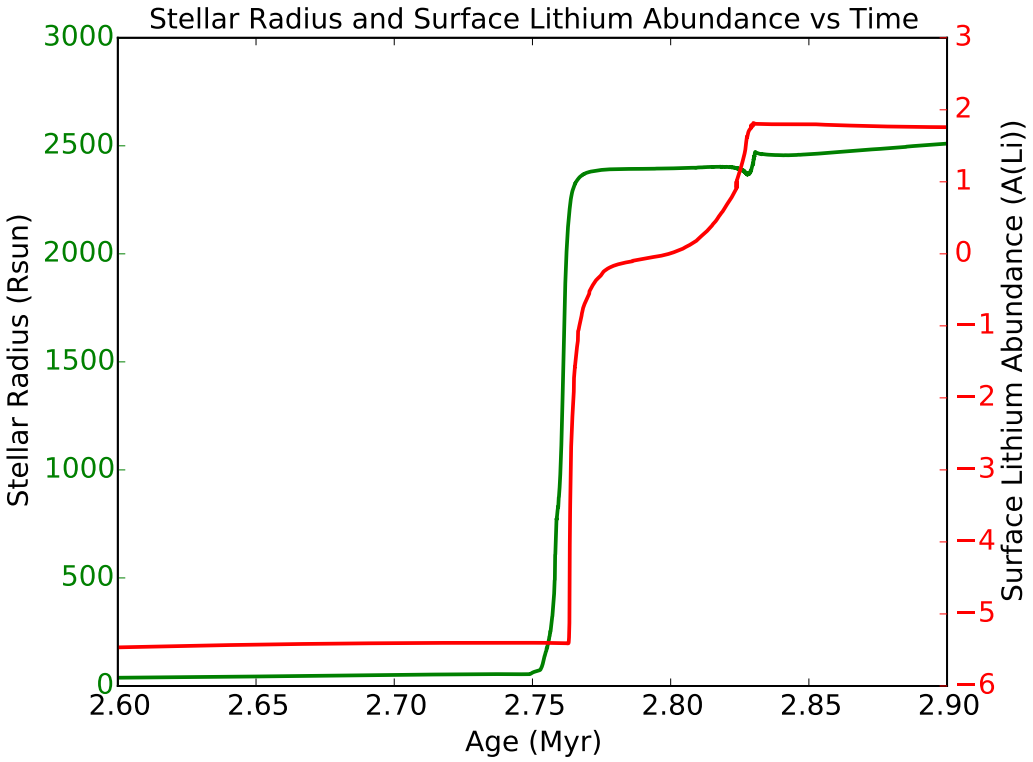


Figure 23: Lithium production (A(Li)) in red and Radius of star in solar units in green versus time, zoomed in to the start of core helium burning for a star of initial mass 74 $M_{\odot}$.

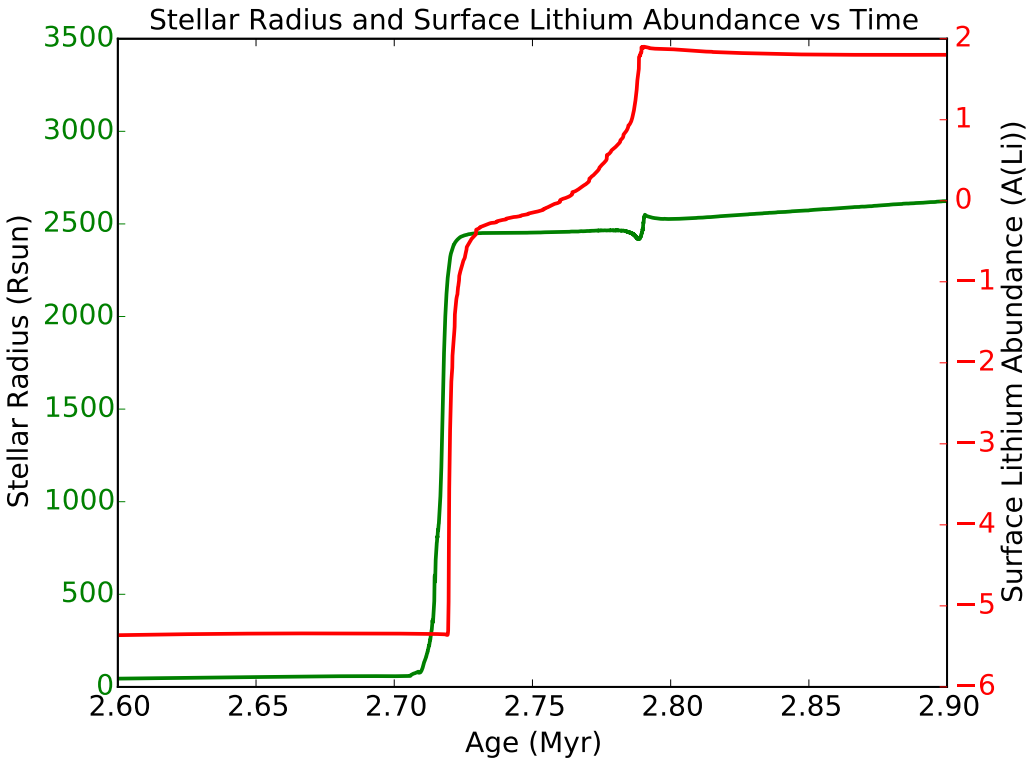


Figure 24: Lithium production (A(Li)) in red and Radius of star in solar units in green versus time, zoomed in to the start of core helium burning for a star of initial mass 77 $M_{\odot}$.

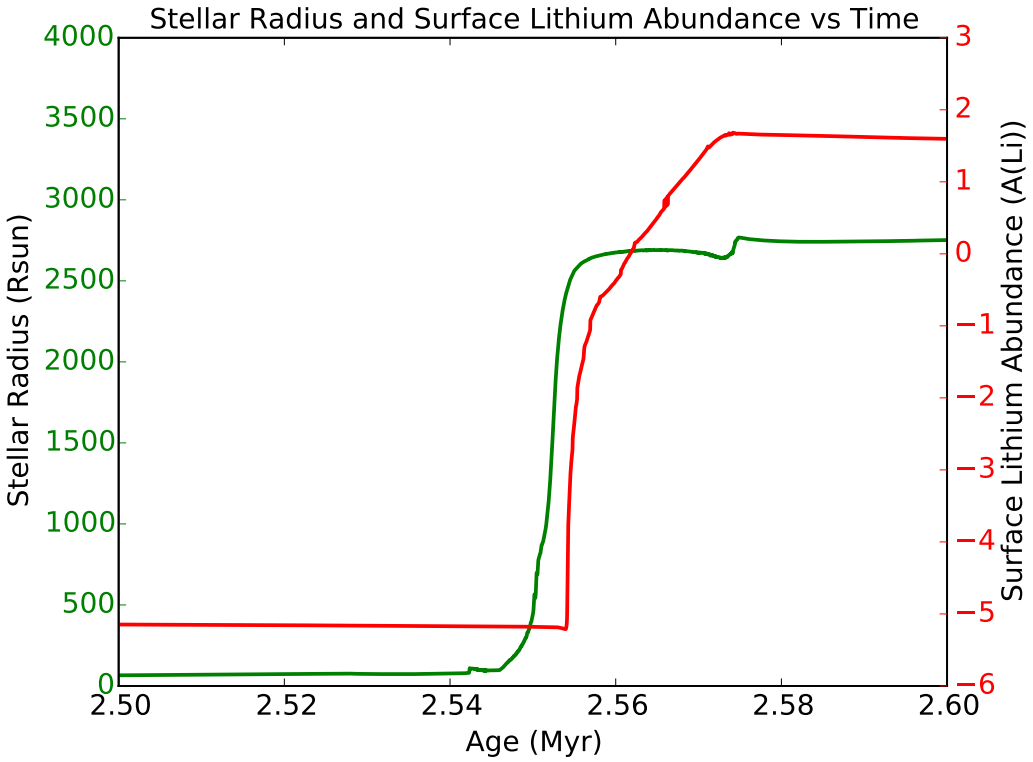


Figure 25: Lithium production (A(Li)) in red and Radius of star in solar units in green versus time, zoomed in to the start of core helium burning for a star of initial mass 88 $M_{\odot}$.

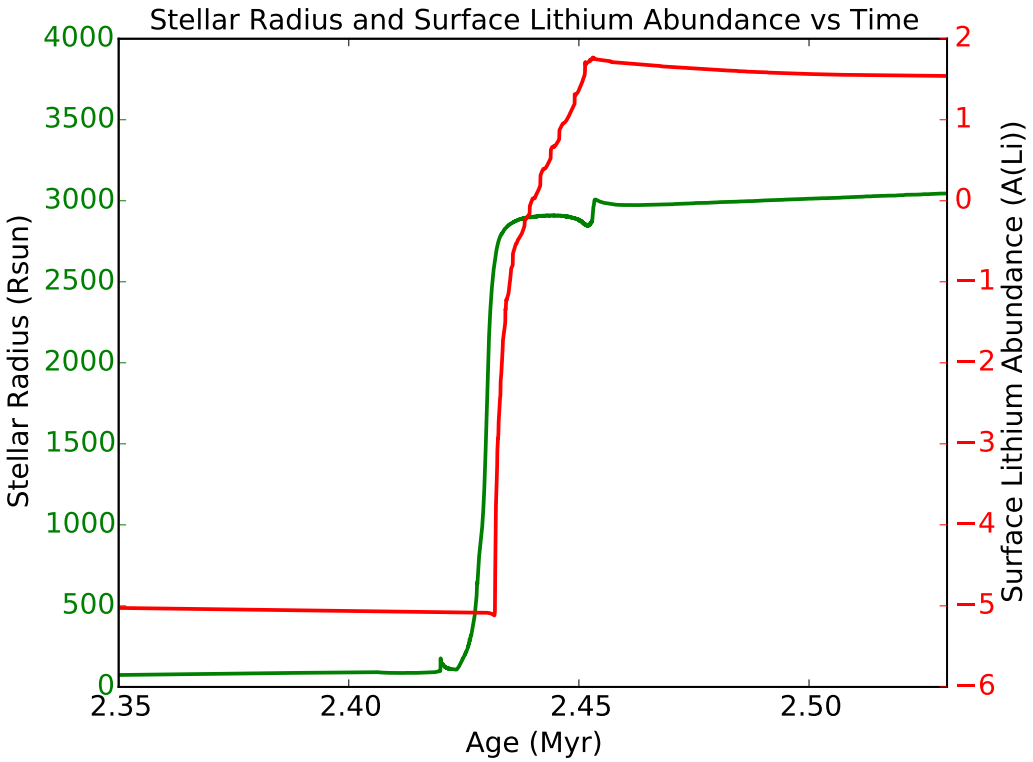


Figure 26: Lithium production (A(Li)) in red and Radius of star in solar units in green versus time, zoomed in to the start of core helium burning for a star of initial mass 100 $M_{\odot}$.

## A.6 Surface Helium Abundance

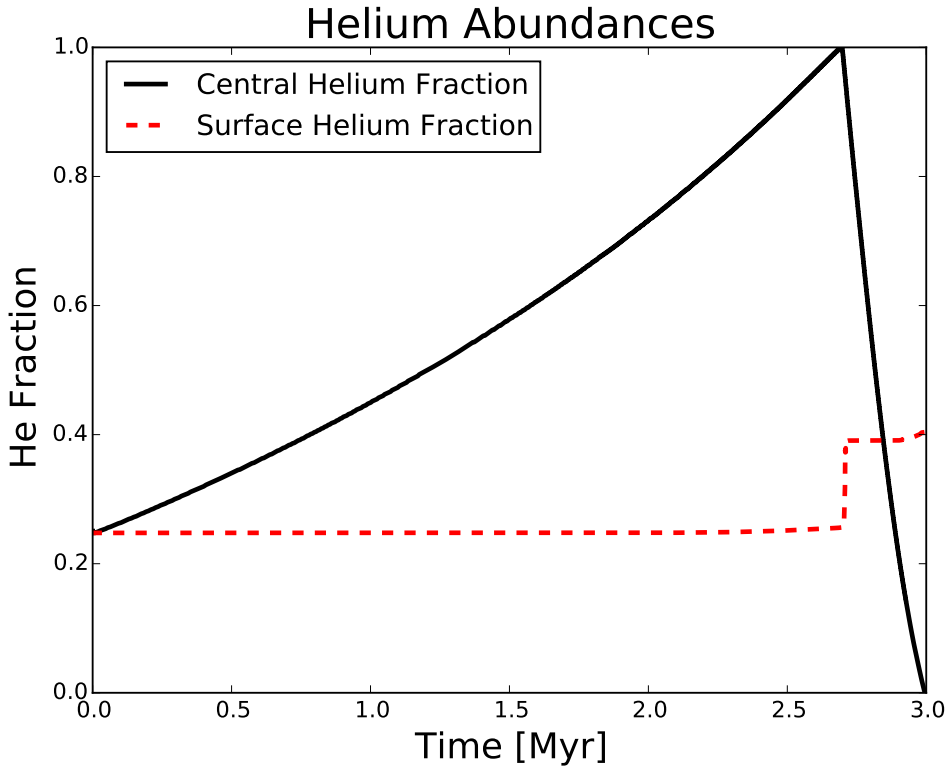


Figure 27: Surface and core helium abundance for a model of initial mass 77 $M_{\odot}$ and initial rotational velocity $75 kms^{-1}$.

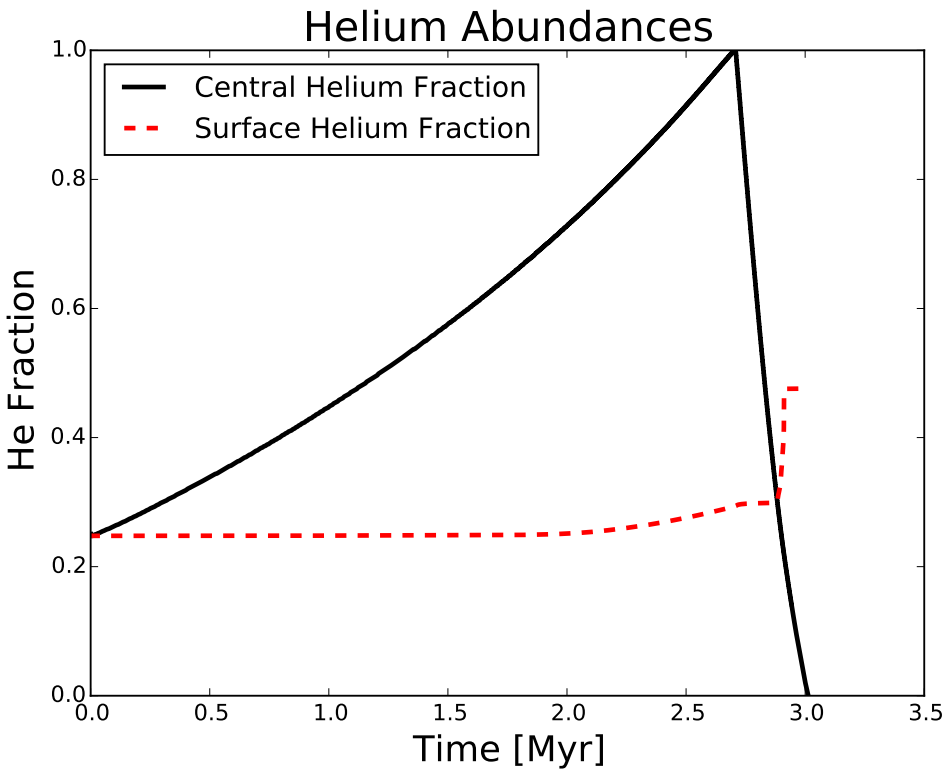


Figure 28: Surface and core helium abundance for a model of initial mass 77 $M_{\odot}$ and initial rotational velocity $125 kms^{-1}$.

In Figure 27 and 28 the surface helium abundance can be seen to be higher for the model with higher rotational velocity. This helium increases opacity and hence results in a higher surface temperature.